A study on the determination of mechanical properties of a power law material by its indentation force-depth curve

Jiaming Luo, Jianguo Lin, Trevor Dean

A study on the determination of mechanical properties of a power law material by its indentation force-depth curve

Journal:	*Philosophical Magazine & Philosophical Magazine Letters*
Manuscript ID:	TPHM-05-Nov-0520
Journal Selection:	Philosophical Magazine
Date Submitted by the Author:	22-Nov-2005
Complete List of Authors:	Luo, Jiaming; University of Birmingham, Mechanical Engineering Lin, Jianguo; University of Birmingham, Mechanical and Manufacturing Engineering Dean, Trevor; University of Birmingham, Mechanical and manufacturing Engineering
Keywords:	indentation, finite-element modelling, mechanical properties, numerical simulation
Keywords (user supplied):	Strain hardening, Optimisation

A study on the determination of mechanical properties of a power law material by its indentation force-depth curve

J LUO, J LIN* and T A DEAN

Department of Manufacturing and Mechanical Engineering, School of Engineering, University of Birmingham, Edgbaston, Birmingham, B15 2TT, UK

Abstract: In this study a novel optimisation approach is proposed to extract mechanical properties of a power law material whose stress-strain relationship may be expressed as a power law from its given experimental indentation *P-h* curve. A set of equations have been established to relate the *P-h* curve to mechanical properties, E, σ_y and n, of the material. For the loading part of a *P-h* curve, this approach is based on the assumption that the indentation response of an elastic-plastic material is a linear combination of the corresponding elastic and elastic-perfect plastic materials. For the unloading part of the *P-h* curve, it is based on the assumption that the unloading response of the elastic-plastic material is a linear combination of the full contact straight line and the purely elastic curve. Using the proposed optimisation approach, it was found that the mechanical properties of an elastic-plastic material usually cannot be decided uniquely by using only a single indentation *P-h* curve of the material. This is because in general a few matched sets of mechanical properties were found to produce a given *P-h* curve. It is however possible to identify the best matched set of mechanical properties by knowing some background information of the material. If the best matched material is identified, the predictions of mechanical properties are quite accurate.

Keywords: Instrumented indentation; Mechanical properties; Finite element simulation; Optimisation; Metals; Strain hardening

1 Introduction

Compressive forces are normally used to form micro-components through micro-forming. However, it is difficult to determine material properties via compressive tests of micro-scale materials. Thus micro- or

nano-indentation tests are often used for this purpose. Recent technological advances have led to the general availability of depth-sensing instrumented indentation experiments in micro- and nano- scales [1-9]. These tests provide accurate measurements of the continuous variation of indentation force, P, down to μN, as a function of the indentation depth, h, down to nm. In addition to the determination of traditional hardness, experimental investigations and theoretical/computational studies of indentation have been conducted on many material systems in order to systematically extract material properties from P versus h curves (P-h curves) obtained from instrumented indentation [5, 6, 8, 9, 10-14]. Instrumented indentation has been recently used to study the deformation mechanisms at dislocation-level [15, 16].

Sharp indenters widely used for micro- and nano- indentation tests are of Berkovich or Vickers types. In the simulation community, they are often simplified to a conical sharp indenter with an included half angle, θ, of 70.3° [1]. This angle is chosen since the projected area/depth ratio of the two-dimensional (axisymmetrical) cone is the same as that for the Berkovich or Vickers indenters and a general finding is that computational P-h responses of the conical, Berkovich and Vickers indentations are virtually identical if they have a same projected area/depth ratio. The contact geometry of a conical indenter with a material is shown in Fig. 1, where θ is the included half angle of the conical indenter and a_c and h_c are the contact radius and depth, respectively. Fig. 1 shows the pile-up impression of the indentation where $h_c > h_m$, and h_m is the depth at the maximum load. Dependent on the mechanical properties, there are cases of sink-ins where $h_c < h_m$.

A schematic illustration of a typical P-h curve is shown in Fig. 1. During loading, the response generally follows the relation described by Kick's Law,

$$P = Ch^2 \qquad (1)$$

where C is a constant depending on the geometry of the indenter tip and workpiece material properties. The average contact pressure, $P_{av}=P_m/A_m$ (A_m is the true projected contact area measured at the maximum load P_m), is defined to be the hardness of the indented material. The maximum indentation depth h_m occurs

at P_m, and the initial unloading slope is defined as $S = \left.\frac{dP_{ul}}{d_h}\right|_{h_m}$, where P_{ul} is the unloading force. The residual indentation depth after complete unloading is h_r. As discussed by Giannakopoulos and Suresh [13], C, S and h_r/h_m are three independent characteristic parameters that can be directly obtained from a single P-h curve. These characteristic parameters have been used to determine elastic-plastic properties of the indented materials and will be discussed in more detail later.

For many pure and alloyed engineering metals, their plastic behaviour can be closely approximated by a power law description [17], as shown schematically in Fig. 2. A simple elastic-plastic, true stress–true strain behaviour is assumed to be

$$\sigma = \begin{cases} E\varepsilon & for\ \sigma \le \sigma_y \\ R\varepsilon^n & for\ \sigma \ge \sigma_y \end{cases} \quad (2)$$

where E is the Young's modulus, R a strength coefficient, n the strain hardening exponent, σ_y the initial yield stress. For $\sigma > \sigma_y$, one can approximately express:

$$\varepsilon = \varepsilon_y + \varepsilon_p \quad (3)$$

where ε_y is strain at yield stress and ε_P is the plastic strain, then

$$\sigma = \sigma_y (1 + \frac{E}{\sigma_y}\varepsilon_p)^n \quad (4)$$

Therefore, to describe the mechanical properties of a power law material, three quantities, E, σ_y and n are needed. A lot of efforts have been made in the recent few years to derive approaches to extract these mechanical properties from a single or multi-set of P-h curves, and will be briefly reviewed in the following sections.

1.1 Loading part of a *P-h* curve

It has been shown by many numerical simulations [8, 9, 11, 14, 18-22] that Eq.(1) is a good approximation for elastic, elastic–perfect plastic and elastic–plastic materials. The results obtained by the finite element (FE) analysis [18] is cited below, which considered a sharp Berkovich indentation on an elastic material,

$$P = f(\nu)Eh^2 \tag{5}$$

where

$$f(\nu) = 2.1891(1 - 0.21\nu - 0.01\nu^2 - 0.41\nu^3)\frac{1}{1-\nu^2} \tag{6}$$

and that on an elastic–plastic material,

$$P = \frac{1.273}{(\tan 24.7°)^2}(1 + \frac{\sigma_{0.29}}{\sigma_y})(1 + \ln\frac{E\tan 24.7°}{3\sigma_y})\sigma_y h^2 \tag{7}$$

where ν is Poisson's ratio, $\sigma_{0.29}$ is the so-called representative stress corresponding to a representative strain of 0.29 defined by Giannakopoulos and Suresh [13], and the ratio $\sigma_{0.29}/\sigma_y$ is an indicator of the strain-hardening property of materials.

1.2 Unloading curve and Young's modulus

The Young's modulus E can be estimated from the unloading curve which is assumed to be purely elastic. For a body of revolution, an analytical model suggested by Sneddon [23] relates the slope at the beginning of the unloading, S, the reduced modulus, E^*, and the projected contact area, A_m (Fig. 1):

$$E^* = \frac{1}{\alpha\sqrt{A_m}}S \tag{8}$$

where E^* is defined by:

$$\frac{1}{E^*} = \frac{1-\nu^2}{E} + \frac{1-\nu_i^2}{E_i} \tag{9}$$

E_i, ν_i and E, ν being the Young's modulus and the Poisson's ratio of the diamond indenter and the specimen, respectively. The constant α in Eq.(8), determined from linear-elastic analysis, is dependent on indenter geometry and given by King [24] as α = 1.167 for the Berkovich indenter, 1.142 for the Vickers indenter and 1.128 for the conical indenter with included half angle θ = 70.3°. A recent FE large deformation elasto-plastic analysis conducted by Dao *et al* [1] showed that α is 1.2370 for the Berkovich indenter, 1.2105 for the Vickers indenter and 1.1957 for the conical indenter with θ = 70.3°.

There are two main approaches to determine S and A_m in Eq.(8). The first one is the linear curve fitting method developed by Doerner and Nix [5], who, based on the assumption that the contact area remains unchanged during unloading, proposed that Sneddon's flat punch solution [23] could be used to describe the unloading curve,

$$P = S(h - h_c) \tag{10}$$

where h_c is the true contact indentation depth which takes the pile-up or sink-in into account. The best-fit results of S and h_c depend on the portion of the unloading curve that is employed in the fitting, and it is suggested by Doerner and Nix [5] that the top one-third of the unloading data should be used.

Doerner and Nix's method in Eq.(10) can describe well the unloading behavior of most metals, but often fails to capture that of hard materials such as ceramics. In order to resolve this issue, Oliver and Pharr [6,25] introduced another method, taking into account the large elastic recovery during the unloading process of hard materials. A major contribution of the method is that the unloading part of a *P-h* curve is nonlinear due to the gradual reduction of contact area caused by elastic recovery. In their scheme, the power-law relation,

$$P = B(h - h_r)^m \tag{11}$$

is adopted to fit the whole unloading curve where B and m are the fitting parameters. After the parameters B and m are determined, the unloading slope at the maximum load can be evaluated to be,

$$S = mB(h_m - h_r)^{m-1} \tag{12}$$

Another major difference between Doerner and Nix's and Oliver and Pharr's methods is the approaches to determine the contact area at the maximum load. Given the included half angle, θ, of the conical indenter, the contact area, A_m, can be geometrically derived as (see Fig. 1),

$$A_m = \pi a_c^2 = \pi(h_c \tan\theta)^2 \tag{13}$$

Note that a_c and h_c are used here to represent the contact radius and depth at the maximum load (it was also used to represent the contact radius and depth during unloading in Fig. 1). In Doerner and Nix's method [5], h_c is equal to the fitting parameter h_c in Eq.(10). In Oliver and Pharr's method [6, 25], h_c is taken to be:

$$h_c = h_m - \lambda \frac{P_m}{S} \qquad (14)$$

where the geometric constant λ is taken to be 0.72 for the conical indenter. Since h_c obtained by Doerner and Nix's, Eq.(10), and Oliver and Pharr's methods, Eq.(14), is always smaller than h_m, they can only explain the sink-in expressions. More recently, Giannakopoulos and Suresh [13] proposed that the contact area could be expressed as a polynomial function of the depth ratio h_r/h_m. A more systematic analysis of the piling-up or sinking-in behaviour of elastic-plastic materials under a sharp indentation has been recently given in ref. [26].

1.3 Dimensional analysis and universal functions

Cheng *et al* [9, 8] and Tunvisut et al. [27] have used dimensional analysis to propose a number of dimensionless universal functions, with the aid of computational data points calculated via the FE method. For this approach, one of the most complete studies has been published recently by Dao *et al*. [1]. FE simulations in connection to experiments on aluminium alloys have been used to develop a forward and reverse analysis of sharp indentations on metals. A set of closed-form dimensionless functions was constructed to characterize indentations with a Vickers or a Berkovich pyramid or a conical indenter (θ = 70.3°). Using these functions, the relationships between characteristic parameters, C, *S* and h_r/h_m, of a *P-h* curve and the mechanical properties of a material, *E*, σ_y and *n*, have been set up and then were used to extract mechanical properties of power-law materials by co-equation solving. The method gives very good results in the determination of the Young's modulus *E* and the representative stress corresponding to a value of strain of 0.033, $\sigma_{0.033}$. On the other hand, their analysis is less precise for determining the strain hardening coefficient *n*. For a value of *n* = 0.08 obtained with the tensile test, this method gave a mean value of 0.104 with values ranging from 0 to 0.298. Even if the mean value gives a good estimate of the expected value, the errors are high and at least six experimental curves on the same material were required.

1.4 Zeng and Chiu approach

Most approaches proposed in the literature to determine *E*, σ_y and *n* of a power-law material are all based on the characteristic parameters of a *P-h* curve, namely C, *S* and h_r/h_m. An exception is the work by Zeng *et al* [28] based on empirical observations, which proposes to link the indentation–unloading curve to Young's

modulus and strain-hardening properties. Zeng and Chiu noted that for a general elastic–plastic material, the stress–strain relation is between two extreme cases: purely elastic and elastic perfect–plastic. For a purely elastic material, the indentation–unloading curve will be identical to the loading one as described in Eq.(5). The indentation–unloading curve of an elastic–perfect plastic material, on the other hand, can be approximately described as a straight line depicted in Eq.(10). Thus, the indentation–unloading curve of the general elastic–plastic material will also be between a parabolic curve and a straight line, and can be expressed as,

$$P_{\text{ep\_ul}} = (1-W)P_e + WP_{epp\_ul} \tag{15}$$

where P_{ep_ul}, P_e and P_{epp_ul} represent the loads during indentation-unloading of the elastic-plastic material, purely elastic material with the same E as the elastic-plastic material (obtained by Eq.(5)), and the elastic-perfect plastic material with the same E and σ_y as the elastic-plastic material (obtained by Eq.(10)), respectively. The terms, (1-W) and W, respectively, are the weights of the elastic and the elastic–perfect plastic responses in the unloading curve of the elastic-plastic material. For a Vickers indenter, the depth-projected area function is,

$$A_m = 24.56h_c^2 \tag{16}$$

Note Eq.(16) is the Vickers indenter version of Eq.(13) which is for a conical indenter. Assuming the indenter is rigid, the following equation can be derived by substituting Eq.(16) into (8), solving for S and then substituting the result into Eq.(10), and then substituting Eqs (5), (10) into Eq.(15)

$$P_{\text{ep\_ul}} = (1-W)f(\nu)Eh^2 + 2W\sqrt{\frac{24.56}{\pi}}\frac{E}{1-\nu^2}h_c(h-h_c) \tag{17}$$

Zeng *et al* [28] also relate the weight factor W to strain hardening using the following equation,

$$W = \frac{\sigma_y}{\sigma_{0.29}} \tag{18}$$

They then optimise W, E and h_c in Eq.(17) to fit this equation to the nano-indentation experimental results of 14 different materials in which the Young's modulus ranges from 3 to 650 GPa and the hardness ranges from 0.1 to over 30 GPa. It is found that this fitting scheme can fit the upper half the unloading curve well. Then by combining Eq.(18) and Eq.(7), the yield stress and strain hardening is determined. They found

that the optimised Young's modulus and yield stress derived from the new method agreed well with the values found in literature, but the correctness of strain hardening was not assessed.

Overall, the approaches proposed in the literature to extract E, σ_y and n are mostly based on the characteristic parameters of a P-h curve, namely C, S and h_r/h_m except the approach by Zeng *et al* [28]. It may be imagined that if all the data of the entire loading and unloading indentation P-h curve are used to extract the mechanical properties of a material, E, σ_y and n, the estimation accuracy might be improved. Based on this concept, a new approach to extract E, σ_y and n of a power-law material is proposed in this paper using the FE simulation results of representative materials.

2 Development of a new optimisation approach for determination of mechanical properties

2.1 Numerical model

Axisymmetric FE models were constructed to simulate the indentation response of elastic-plastic solids using the commercial FE code ABAQUS. The conical indenter of included half angle of 70.3° is modelled using a rigid surface. Fig. 3(a) shows the FE model for axisymmetric calculations. The semi-infinite substrate of the indented solid was modelled using 9600 four-noded, bilinear axisymmetric quadrilateral elements, where a fine mesh near the contact region and a gradually coarser mesh further from the contact region were designed to ensure numerical accuracy. To reduce the effect of mesh distortion, self-adaptive mesh control of ABAQUS/explicit was used. At the maximum load, the minimum number of contact elements in the contact zone was no less than 35 in each FEM computation. The mesh was well-tested for convergence and was determined to be insensitive to far-field boundary conditions. An example of the self-adaptive mesh and the Mises stress contour at the maximum load is shown in Fig. 3(b).

A parametric study of 44 cases was conducted (see Table 1 for a complete list of parameters), including 7 cases of purely elastic materials and 8 cases of elastic-perfect plastic materials. These cases represented the range of parameters of mechanical behaviour found in common engineering metals: that is, Young's

modulus E ranged from 30 to 210 GPa, yield strength σ_y from 30 to 2000 MPa, strain hardening exponent n from 0 to 0.5, and Poisson's ratio ν was fixed at 0.3.

2.2 The approach

To extract E, σ_y and n, it is believed that if the entire loading and unloading indentation P-h curve, instead of only using characteristic parameters of a P-h curve, is used, the estimation accuracy will be improved. To realise this strategy, it is necessary to construct functions to relate the loading and unloading parts of a P-h curve to mechanical properties of a material.

2.2.1 The loading curve

2.2.1.1 *Loading curves for elastic and elastic-perfect plastic materials*

The simulation results of seven purely elastic cases showed that the load curves (same as the unloading curves) for purely elastic materials can be expressed as:

$$P_e(E^*,h) = C_e(E^*)h^2 = C_0 E^* h^2 \quad (19)$$

To obtain C_e, a fitting scheme is needed to fit the FE results. C_e is decided for each FE case using a least square fitting scheme, and the C_e vs E^* relationship is shown in Fig. 4 and detailed by Eq.(A1) in Appendix A. C_0 is determined to be 1.9464.

For elastic-perfect plastic materials, it was found that their loading curves can be expressed as:

$$P_{epp\_L}(E^*,\sigma_y,h) = C_{epp\_L}(E^*,\sigma_y)h^2 \quad (20)$$

C_{epp_L} is obtained by fitting the loading part of the P-h curve, using a least square fitting scheme for each elastic-perfect plastic case and is shown in Table 1. The relationship between C_{epp_L} and mechanical properties of materials is then obtained by least square fitting and is expressed by Eq.(A2) in Appendix A. The relationship between C_{epp_L} (Original) and C_{epp_L} (Predicted) is shown in Fig. 5, indicating a high accuracy of Eq.(A2) in Appendix A to calculate C_{epp_L}.

2.2.1.2 *Loading curves for elastic-plastic materials*

The FE simulated *P-h* loading curves for a set of elastic P_e, (E=210GPa), elastic-plastic $P_{ep\text{-}L}$, (E=210GPa, σ_y=900MPa, n=0.3) and elastic-perfect plastic $P_{epp\text{-}L}$, (E=210GPa, σ_y=900MPa, n=0) materials are shown in Fig. 6. Note that the *P-h* curve for an elastic-plastic material, $P_{ep\text{-}L}$, is always between the curves for elastic, P_e, and elastic-perfect plastic materials, $P_{epp\text{-}L}$. Thus *P-h* curve for elastic-plastic material is assumed to be a linear combination of the corresponding elastic and elastic-perfect plastic materials,

$$P_{ep\_L} = (1 - W_L)P_e + W_L P_{epp\_L} \tag{21}$$

Where the terms, (1-W_L) and W_L, are the weights of the elastic and the elastic–perfect plastic responses in the loading curve of the elastic-plastic material. W_L is a function of mechanical properties of the elastic-plastic material. Using Eq.(1), (19) and (20), the following expression can be obtained:

$$W_L(\frac{E^*}{\sigma_y}, n) = \frac{\mathrm{C_e}\text{-}\mathrm{C_{ep\_L}}}{\mathrm{C_e}\text{-}\mathrm{C_{epp\_L}}} \tag{22}$$

Where C_{ep_L} is obtained by fitting the loading part of the *P-h* curve of each elastic-plastic material and is shown in Table 1 together with the resultant W_L. It was found that this weighting scheme worked very well. An example is shown in Fig. 6 for an elastic-plastic material of E=210GPa, σ_y=900MPa, n=0.3. The parameters C_e, C_{epp_L}, C_{ep_L} and W_L were determined to be 449,163, 156,603, 250,754 and 0.6782, respectively. Using the least square fitting scheme, the relationship between W_L and mechanical properties is given in Eq.(A3) in Appendix A. The relationship between W_L (Original) and W_L (Predicted) was obtained and is shown in Fig. 7, indicating a high accuracy of Eq.(A3) in Appendix A in calculating W_L.

2.2.2 The unloading curve

Zeng and Chiu's weighting scheme as described in section 1.4 is firstly used in an attempt to describe the indentation-unloading curve (in fact, the upper 50% of the unloading curve) of an elastic-plastic material by weighting the unloading curves of the corresponding elastic and elastic-perfect plastic materials. For conical indenter, using Eq.(8) and Eq.(13), Eq.(17) becomes:

$$P_{\mathrm{ep\_ul}} = (1 - W)C_e h^2 + W\alpha\sqrt{\pi}(\tan\theta)\frac{E}{1-\nu^2}h_c(h - h_c) \tag{23}$$

Then this equation is used to optimise W, E, and h_c, to fit the FE simulation results using the method described by Zeng and Chiu [28]. An example is given in Fig. 8 which shows the best results of the upper 50% unloading curves of two materials - same E (210GPa) and σ_y (900MPa), but different n (0.1 and 0.5). It was found that this weighting scheme worked well for high strain hardening materials, but unsatisfactorily for low strain hardening materials.

The difficulties of Zeng and Chiu's fitting scheme may be due to the fact that they used a straight line, Eq.(10), for the elastic-perfect plastic material. In fact, careful investigation of unloading curves showed that the straight line assumption is not held even for unloading of elastic-perfect plastic materials. Detailed FE model investigation of the unloading process indicated that the contact area gradually decreases after a short period of initial full contact during unloading process, even for elastic-perfect plastic materials. It is the reduction of contact area that causes the unloading curve to deviate from a straight line. Based on this understanding, a new fitting scheme is proposed for the unloading curve.

As shown in Fig. 9, if the contact area does not change during unloading, the unloading curve would be a straight line, P_{fc}, with a slope at the maximum load (note this is different from the straight line for the corresponding elastic-perfect plastic material as proposed in Zeng and Chiu's method). However, a reduction of the contact area is inevitable at some stage and the unloading curve will deviate from the straight line. Note that for purely elastic materials, the reduction of contact area is continuous. Therefore, the reduction of contact area of an elastic-plastic material can be thought of as having some kind of similarity to the corresponding purely elastic material. The unloading response of the elastic-plastic material should be a combination of the full contact straight line and the purely elastic curve. It is proposed that the unloading curve of an elastic-plastic material is a linearly weighted addition of the elastic material response and the full contact straight line. As shown in Fig. 9, to use the weighting scheme, the P-h curve for the purely elastic material is translated downward to meet the maximum load point for the elastic-plastic material so that the modified P-h curve for the purely elastic material is

$$P_{em} = P_e - \Delta P = C_0 E^* h^2 - (C_0 E^* h_m^2 - P_m) \qquad (24)$$

where ΔP is the difference between the maximum load of the purely elastic and elastic-plastic materials. The full contact straight line is

$$P_{fc} = S(h - h_m) + P_m \quad (25)$$

where S is the slope of the unloading curve at the maximum load and is decided by Oliver and Pharr's methods, Eq.(12). The weighting scheme is then expressed as

$$P_{ep\_ul} = (1 - W_{ul})P_{em} + W_{ul}P_{fc} \quad (26)$$

For each unloading case, the least square fitting scheme was used to find the optimised W_{ul} and the result is shown in Table 1. It was found that excellent fitting can be obtained for at least the upper 50% of the unloading curve by the proposed weighting scheme. For the two materials shown in Fig. 8, the fitting results for the upper 50% unloading curves are shown in Fig. 10, indicating an excellent fitting. W_{ul} is determined to be 0.92 and 0.84 for the two materials: n=0.1 and 0.5, respectively. However, it has to be pointed out that the proposed weighting scheme cannot fit the entire unloading curve well and this is shown in Fig. 11 for the n=0.5 material in Fig. 10.

Using the least square fitting scheme, the relationship between W_{ul} and mechanical properties is obtained and given in Eq.(A4) in Appendix A. The relationship between W_{ul} (Original) and W_{ul} (Predicted) is shown in Fig. 12, indicating a reasonable accuracy of Eq.(A4) in Appendix A to predict W_{ul} (note, however, that the accuracy of Eq.(A4) to predict W_{ul} is not as good as that of Eq.(A3) to predict W_L).

2.2.3 The residual depth

An important characteristic parameter of the P-h curve is the residual depth, h_r, after complete unloading (also shown in Table 1 for each simulation case). The residual depth is related to mechanical properties of the material as:

$$\frac{h_r}{h_m} = \varphi(n, \frac{E^*}{\sigma_y}) \quad (27)$$

Following the same least square fitting approach used in previous sections, Eq.(27) was determined and shown in Eq.(A5) in Appendix A. The high accuracy of Eq.(A5) in predicting h_r/h_m is shown in Fig. 13.

2.3 The extraction of mechanical properties from *P*-h curves using an optimisation approach

With the loading and unloading parts of a *P-h* curve being related to the mechanical properties of a material by Eq.(21) and (26), respectively, the mechanical properties of the matereial are determined by minimising the errors between the FE (experimental) and predicted (using Eq.(21) and (26)) *P-h* curves, as shown in Fig. 14. An objective function for the optimisation is formulated as:

$$Min\left\{\sum_{i=1}^{N_1}[P_{ep\_L,i}^{FE}-P_{ep\_L,i}^{Predicted}(E^*,\sigma_y,n)]^2+\sum_{j=1}^{N_2}[P_{ep\_ul,j}^{FE}-P_{ep\_ul,j}^{Predicted}(E^*,\sigma_y,n)]^2+[S(h_r^{FE}-h_r^{Predicted}(E^*,\sigma_y,n))]^2\right\} \quad (28)$$

where $P_{ep\_L,i}^{Predicted}$ and $P_{ep\_ul,j}^{Predicted}$ are calculated by Eq.(21) and (26), respectively. h_r^{FE} is the residual depth obtained by FE simulations or experiments, $h_r^{Predicted}$ is the residual depth predicted by Eq.(27). The detailed definitions of the parameters in the above equations are given in Fig. 14. The first term in the equation defines the errors in the loading phase and the second in the unloading. N_1 and N_2 represent the data points in the loading phase and the upper 50% of unloading phase, respectively. The third term is introduced to enhance the convergence at the last stage of the unloading phase to overcome, at least partially, the problem that the lower 50% of the unloading phase cannot be described by Eq.(26). S is a weighting factor to deal with scaling problem and is taken as the slope of the unloading curve at the maximum load point.

For a particular set of *P-h* data (obtained experimentally or by FE simulation as is the case in this study), the Bates and Watts' optimisation method [29], is used to determine the mechanical properties of the material by minimising the residual defined in Eq.(28). The Bates and Watts' optimisation method improves the efficiency of optimisation by normalising optimised parameters in situations where several parameters, which have different magnitude but are confined within their own individual boundaries, need to be optimised. For a parameter to be optimised, c_i, with upper and lower boundaries of fixed values, L_i and U_i, it is converted to parameter ϕ_i by:

$$c_i = L_i + \frac{U_i - L_i}{1+e^{-\phi_i}} \quad (29)$$

where ϕ_i is a new parameter corresponding to c_i, and can take any value between $-\infty$ and $+\infty$. For Eq.(28), c_i represents E^*, σ_y and n, and the corresponding ϕ_i now have identical range of value (i.e. $-\infty$ and $+\infty$). Case studies are carried out next.

3 Case studies-effectiveness of the proposed optimisation approach

To use The Bates and Watts' optimisation method [29], the lower and upper boundaries of the parameters to be optimised have to be defined. Here the optimisation parameters are the mechanical properties of the material of concern. For a material without any known background information, wider search ranges have to be used. In this study, ranges of E, σ_y and n are taken to be 10 to 250 GPa, 10 to 2500MPa and 0 to 0.5, respectively, since most metals will have their mechanical properties in these ranges. However, in most cases, some background information of the material of concern should be given. In particularly, since Young's modulus is less affected by material processing, it would be able to be confined in a narrow range or a fixed value. In this study, optimisation is also conducted for fixed Young's modulus values, reducing the optimisation parameters in Eq.(28) to two: σ_y and n. Two methods were used to decide the Young's modulus. One was to assume it is known. The other was to obtain the value by using Oliver and Pharr's method, see section 1.2.

Another problem with the Bates and Watts' optimisation method is how to choose the initial values of the optimisation parameters. To ensure a comprehensive search of all the minimum vortexes of the objective function, each ϕ_i (here i stands for E, σ_y and n) in Eq.(29) is allowed to change from -9 to 9 with a step length of 3 for three parameter optimisation (i.e. E, σ_y and n are all optimised), and from -10 to 10 with a step length of 1 for two parameter optimisation (i.e. σ_y and n are optimised). This means that for three parameter optimisation, a total of 7×7×7=343 sets of initial values are used, while for two parameter optimisation, a total of 21×21=441 sets of initial values are used.

Typical optimisation results are shown in Table 2 for four FE simulated materials, which gives the true material properties, optimisation boundaries for E (note boundaries for σ_y and n are fixed to be 10 to

2500MPa and 0 to 0.5 for all cases), optimised mechanical properties and the residuals of the objective function. The optimisation case which best matches the original material is heavily bordered.

In general, for each given set of optimisation parameter boundaries, more than one minimum vortexes are found. The number of the matched sets of material properties whose residuals are not more than 10% of the global minimum is given in Table 2. Table 2 also lists up to three sets of matched material properties when there are more. Ideally the best matched set of mechanical properties should correspond to the global minimum. Unfortunately this is sometimes not the case. For those vortexes having residual values of the objective function very close to the global minimum, in practice they can be thought of as being virtually equal in consideration of the approximation of optimisation algorithm. To prove that each set of optimised mechanical properties give similar *P-h* curves as the original materials, indentation of each optimised material is FE-simulated again. Examples for E=210GPa, σ_y=900MPa, n=0.3 material are shown in Fig. 15. All other materials follow the same trend. This figure indicates that a particular experimental (or FE simulation) *P-h* curve can be produced by a few sets of material properties, i.e. a few materials, and the difference should be within experimental error in real measurements. This means that without any background information of the material of concern, the mechanical properties of the material cannot be uniquely decided by a single indentation *P-h* curve. Because of the multiplicity of the optimisation results, the background information of the material of concern must be used to choose the best matched optimised material (heavily bordered in Table 2). For three parameter optimisation, it was found the best matched optimisation generally predicts the Young's modulus more accurately than Oliver and Pharr's method [6] (maximum error 2% for optimisation approach vs maximum error 22% for Oliver and Pharr's method). The prediction of σ_y is also quite accurate (maximum error 12% for the four materials). However, the prediction of n is not very accurate (maximum error 30%), particularly for lower n values (n<0.2). The prediction accuracy of σ_y and n by the optimisation approach is improved if the Young's modulus is known, as is generally the case of a material in practice, with maximum errors of 12% and 19% for σ_y and n, respectively (compared for the best matched optimisation) for these four materials. Furthermore, it was found that for two parameter optimisation, the number of matched sets of mechanical properties is greatly reduced. In most

cases, a unique solution is found. However, using the Young's modulus predicted by Oliver and Pharr's method in the two parameter optimisation seems not to be a good approach, since Oliver and Pharr's method often overestimates the Young's modulus.

4 Discussion

This study proposes a novel optimisation approach to extract mechanical properties of a power law material from its given experimental (or FE simulation) indentation *P-h* curve. A set of equations have been established to relate the *P-h* curve to the power law material's mechanical properties, E, σ_y and n. For loading part of a *P-h* curve, it is based on the assumption that the indentation response of an elastic-plastic material is the linear combination of the corresponding elastic and elastic-perfect plastic materials. For unloading part of the *P-h* curve, it is based on the assumption that the unloading response of the elastic-plastic material is a linear combination of the full contact straight line and the purely elastic curve.

It was found that in general the optimisation of a given *P-h* curve can find a few matched materials by the optimisation scheme. The FE simulations of all the matched materials proved that they produce similar (if not identical, the difference is within the experimental errors in real measurements) *P-h* curves. This means that mechanical properties of the material of concern cannot be uniquely decided by a single *P-h* curve. Cheng and Cheng [12] also found the non-uniqueness problem by giving accidental examples of matched materials for a given *P-h* curve. The present study shows that the non-uniqueness problem is a commonplace for nearly all *P-h* curves and the matched materials can be found in a deterministic way through optimisation algorithm. For three parameter (i.e. E, σ_y and n) optimisation, although the best matched material is identified in this study (Table 2), it could be difficult to identify it in reality since the material properties are not exactly known, particularly when there is large number of matched materials to choose from. However, it is found that the known information of the material of concern can be used to narrow the search range of the optimisation results. For example, if the Young's modulus is known, a unique material could be found in most cases by two parameter (σ_y and n) optimisation. Once the best matched material is identified, the accuracy of mechanical property predictions is reasonably good. For example, the accuracy of Young's modulus prediction is better than the widely accepted Oliver and Pharr's method

(maximum error 2% for optimisation approach vs maximum error 22% for Oliver and Pharr's method). For the two parameter optimisation (i.e. the Young's modulus of the material is known), the prediction accuracy of σ_y and n is within 12% and 19%, respectively, generally better than other methods in the literature [1], particularly for high n values ($n \geq 0.2$). The increased accuracy of mechanical property prediction can be attributed to the fact that all the *P-h* curve data, except the lower 50% of the unloading curve, are used for the present optimisation approach, instead of only using the characteristic values of the *P-h* curve. Recently, Bucaille *et al* [2] proposed a method to extract plastic mechanical properties of a material by using at least two *P-h* curves of the material obtained for different indenter included angles. Their method is based on the dimensional analysis and universal functions established in Dao's work [1]. The prediction of n value is greatly improved by their multi-angle indentation experimental design. It is believed that if two or more *P-h* curves of a material for different included angles are used in the optimisation scheme, the non-uniqueness problem for the three parameter optimisation could be eventually removed. Further investigation is carried out in this direction.

The prediction accuracy of mechanical properties using the proposed optimisation scheme is obviously dependent on the goodness of Eq.(21), (26) and (27) to relate the loading curve, unloading curve and h_r/h_m to mechanical properties, respectively, since they are basic functions put into the objective function Eq.(28). Fig. 6 and Fig. 7 show that Eq.(21) can relate the loading curve to mechanical properties well, and Fig. 13 shows that Eq.(27) can relate h_r/h_m to mechanical properties well. However, Fig. 12 shows that Eq.(A4) is not very good to relate W_{ul} to mechanical properties, and Fig. 10 and Fig. 11 indicate that Eq.(26) can only be used to relate the upper 50% unloading curve to mechanical properties. During the development procedure of the current optimisation scheme, it was found that the inclusion of the unloading part of a *P-h* curve is very important to lessen the non-uniqueness problem. If only the loading part of a *P-h* cure is used in the objective function, the number of matched materials increases enormously, and matched materials for the loading curve are not guaranteed to produce similar unloading curves. The difficulty in relating the unloading *P-h* curve to mechanical properties is the main factor that affects the prediction accuracy of the proposed optimisation scheme. Therefore, for better optimisation result, it is critical to find a better function

to relate the entire unloading curve to mechanical properties. This is a challenging task because the unloading process of the indenter-material contact is complicated. In particular, the change of contact area during unloading has to be described accurately. Work in this direction is also under investigation.

However, the optimisation scheme even at its current state is good enough in some cases for practical use if users know some background information of the material of concern, particularly when Young's modulus is known. To those readers who are not familiar with optimisation algorithm, this method may appear to be daunting. In fact, all the optimisation calculation in this study is carried out in Microsoft Excel, using the Solver add-in. A simple VBA program is written to search for the matched materials and the comprehensive search need only a few minutes.

5 Conclusions

1. A novel optimisation approach to extract mechanical properties of a power law material from its given experimental (or FE simulation) indentation *P-h* curve is proposed. It was found that the prediction accuracy of material properties can be improved by this approach since the entire *P-h* curve data, except the lower 50% of the unloading curve, are used. This optimisation approach is more effective as it is applied to high strain hardening materials (n is 0.2 or above) at this stage.
2. Using the proposed optimisation approach, it was found that mechanical properties of an elastic-plastic material usually cannot be determined uniquely by using only a single indentation *P-h* curve of the material. This is because in general a few matched set of mechanical properties were found to produce a given *P-h* curve.
3. It is however possible to identify the best matched set of mechanical properties by knowing some background information of the material. In particular, if Young's modulus is known, a unique matched material can be found in most cases. If the best matched material is identified, the predictions of mechanical properties are quite accurate.

6 Acknowledgements

The work described in this paper was supported by a European Union FP6 Integrated Project on Mass-Manufacture of Miniature/Micro Products - MASMICRO (Project No: 500095-2).

Appendix A: Functions

The fitted functions described in the main text body are listed:

$$P_e(E^*,h) = C_e(E^*)h^2 = C_0 E^* h^2 = 1.9464 E^* h^2 \tag{A1}$$

$$\begin{aligned} P_{epp\_L}(E^*,\sigma_y,h) &= C_{epp\_L}(E^*,\sigma_y)h^2 \\ &= \sigma_y \left\{ \begin{array}{l} -0.27531\left[\ln\left(\frac{E^*}{\sigma_y}\right)\right]^3 - 0.21504\left[\ln\left(\frac{E^*}{\sigma_y}\right)\right]^2 + \\ 43.21185\ln\left(\frac{E^*}{\sigma_y}\right) - 98.90853 \end{array} \right\} h^2 \end{aligned} \tag{A2}$$

$$\begin{aligned} & W_L\left(n,\frac{E^*}{\sigma_y}\right) \\ &= \left(-9.6132\times10^{-4} + 1.627\times10^{-1} n - 8.6988\times10^{-2} n^2\right)\ln\left(\frac{E^*}{\sigma_y}\right) + \\ & \quad 1.0053 - 1.203n + 1.0584\times10^{-1} n^2 \end{aligned} \tag{A3}$$

$$\begin{aligned} & W_{ul}\left(n,\frac{E^*}{\sigma_y}\right) \\ &= \left(-7.5834\times10^{-8} - 4.5276\times10^{-7} n + 7.6258\times10^{-7} n^2\right)[\ln(\frac{E^*}{\sigma_y})]^2 + \\ & \quad (8.1967\times10^{-5} + 5.187\times10^{-4} n - 6.4586\times10^{-4} n^2)\ln(\frac{E^*}{\sigma_y}) + \\ & \quad (8.7875\times10^{-1} + 8.6099\times10^{-2} n - 5.134\times10^{-1} n^2) \end{aligned} \tag{A4}$$

$$\begin{aligned} & \frac{h_r}{h_m} = \varphi\left(n,\frac{E^*}{\sigma_y}\right) \\ &= \left(3.971\times10^{-3} - 3.0783\times10^{-3} n - 2.704\times10^{-3} n^2\right)[\ln(\frac{E^*}{\sigma_y})]^3 + \\ & \quad (-8.6249\times10^{-2} + 4.298\times10^{-2} n + 7.8106\times10^{-2} n^2)[\ln(\frac{E^*}{\sigma_y})]^2 + \\ & \quad (0.6419 - 0.11975n - 0.63727n^2)\ln(\frac{E^*}{\sigma_y}) + \\ & \quad (-0.64405 - 0.22042n + 1.27651n^2) \end{aligned} \tag{A5}$$

References

1 M. Dao, N. Chollacoop, K. J. Van Vliet., T. A. Venkatesh, and S. Suresh, Acta mater. **49** 3899 (2001)

2 J.L. Bucaille, S. Stauss, E. Felder and J. Michler, Acta Mater. **51** 1663 (2003)

3 D. Tabor, Hardness of Metals. Clarendon Press, Oxford, 1951

4 D. Tabor, Rev. Phys. Technol., **1** 145 (1970)

5 M. F. Doerner and W. D. Nix, J. Mater. Res., **1** 601 (1986)

6 W. C. Oliver and G. M. Pharr, J. Mater. Res., **7**, 1564 (1992)

7 A. Bolshakov, W. C. Oliver and G. M. Pharr, J. Mater. Res., **11** 760 (1997)

8 Y. -T. Cheng and C. -M. Cheng, J. Appl. Phys., **84** 1284 (1998)

9 Y. T. Cheng and C. -M. Cheng, Appl. Phys. Lett., **73** 614 (1998)

10 S. Suresh, J. Alcala and A. E. Giannakopoulos, US Patent No. 6,134,954, Oct. 24, 2000

11 A. E. Giannkopoulos, P. L. Larsson and R.Vestergaard, Int. J. Solids Struct., **31** 2679 (1994)

12 Y. T. Cheng and C. M. Cheng, J. Mater. Res., **14** 3493 (1999)

13 A. E. Giannakopoulos and S. Suresh, Scripta Mater., **40** 1191 (1999)

14 T. A. Venkatesh, K. J. Van Vliet, A. E. Giannakopoulos and S. Suresh, Scripta Mater., **42** 833 (2000)

15 H. G. M. Kreuzer and R. Pippan, Phil. Mag., **85** 3301 (2005)

16 H. Y. Liang, C. H. Woo, H. C. Huang, A. H. W. Ngan and T. X. Yu, Phil. Mag., **83** 3609 (2003)

17 B. H. Cheong, J. Lin and A. A. Ball, J. Strain Analysis, **35** 149 (2000)

18 P. -L. Larsson, A. E. Giannakopoulos, E. Söderlund, D. J. Rowcliffe and R. Vestergaard, Int. J. Solids Struct., **33** 221 (1996)

19 A. E. Giannakopoulos and P. -L. Larsson, Mech. Mater., **25** 1 (1997)

20 Y. -T. Cheng and C. -M. Cheng, Int. J. Solids Struct., **36** 1231 (1999)

21 Y. -T. Cheng and C. -M. Cheng, Phil. Mag. Lett., **77** 39 (1998)

22 G. G. Bilodeau, J. Appl. Mech., **59** 519 (1992)

23 I. N. Sneddon, Int. J. Eng. Sci., **3** 47(1965)

24 R. B. King, Int. J. Solids Struct., **23** 1657 (1987)

25 G. M. Pharr, W. C. Oliver and F. R. Brotzen, J. Mater. Res., **7** 613 (1992)

26 Z.H. Xu, J. Agren, Phil. Mag., **84** 2367 (2004)

27 K. Tunvisut, N. P. O'Dowd and E. P. Busso, Int. J. Solids Struct., **38** 335 (2001)

28 K. Zeng and C.-h Chiu, Acta mater., **49** 3539 (2001)

29 D. M. Bates and D. G.,Watts, Non-linear Regression Analysis and Its Applications. Wiley, New York, 1988

Table 1 Elastic-plastic parameters used in the present study and some simulation results.

	E (GPa)	σ_y (MPa)	n	C_e, C_{epp_L}, C_{ep_L}	W_L	W_{ul}	h_r/h_m
Elastic	10			21325.9			
	30			64145.7			
	50			106973.7			
	90			192628.4			
	130			278285.1			
	170			363943.3			
	210			448690.6			
Elastic-Perfect Plastic	30	30	0	3014.6	1	0.8886	0.9852
	50	200	0	17636.1	1	0.8856	0.9446
	90	500	0	41584.5	1	0.8931	0.9259
	130	2000	0	120447.5	1	0.8876	0.8326
	210	300	0	29468.6	1	0.9017	0.9792
	210	500	0	47099.1	1	0.8906	0.9654
	210	900	0	78527.4	1	0.8882	0.9409
	210	1800	0	133644.1	1	0.8970	0.8950
Elastic-Plastic	30	30	0.1	3962.3	0.9845	0.8858	0.9808
			0.3	6962.4	0.9354	0.9044	0.9572
			0.5	12533.9	0.8443	0.8597	0.9086
	50	200	0.1	20696.0	0.9657	0.8968	0.9298
			0.3	28544.1	0.8779	0.8822	0.8893
			0.5	39386.1	0.7565	0.8263	0.8210
	90	500	0.1	47305.2	0.9621	0.9103	0.9107
			0.2	54044.6	0.9175	0.9014	0.8905
			0.3	61992.8	0.8649	0.8888	0.8659
			0.4	71182.5	0.8040	0.8625	0.8341
			0.5	81218.2	0.7376	0.8264	0.7953
	130	2000	0.1	128233.2	0.9507	0.8942	0.8126
			0.2	137768.8	0.8903	0.8802	0.7869
			0.3	148221.3	0.8240	0.8625	0.7564
			0.4	159008.1	0.7557	0.8467	0.7193
			0.5	169679.0	0.6881	0.7921	0.6825
	210	300	0.1	38540.9	0.9784	0.9213	0.9715
			0.3	63410.7	0.9190	0.9026	0.9454
			0.5	105627.3	0.8183	0.8701	0.8933
	210	500	0.1	58588.2	0.9714	0.9282	0.9564
			0.3	88173.4	0.8977	0.9074	0.9236
			0.5	133036.6	0.7860	0.8350	0.8641
	210	900	0.1	91676.6	0.9645	0.9155	0.9286
			0.2	107164.9	0.9226	0.8987	0.9096
			0.3	125377.1	0.8734	0.8950	0.8879
			0.4	146703.8	0.8158	0.8743	0.8583
			0.5	170918.4	0.7504	0.8400	0.8204
	210	1800	0.1	147530.0	0.9559	0.8995	0.8764
			0.3	182278.0	0.8456	0.8803	0.8270
			0.5	224175.4	0.7126	0.8305	0.7509

Table 2 Examples of parameters obtained from optimisation.

Material Properties			Range for E (GPa)	No. of matched sets	Chosen sets of optimised values						Residual
E (GPa)	σ_y (MPa)	n			E (GPa)	E%	σ_y (MPa)	σ_y%	n	n%	
90	500	0.1	10-250	20	87	-3	600	20	0.00	-98	0.5650
					90	0	473	-5	0.13	30	0.5465
					113	25	111	-78	0.50	400	0.5465
			90	1	90	0	485	-3	0.12	19	0.5467
			110*	1	110	22	159	-68	0.44	336	0.5514
90	500	0.2	10-250	9	83	-8	736	47	0.00	-100	0.6478
					88	-2	531	6	0.18	-11	0.6260
					107	19	160	-68	0.50	148	0.6283
			90	1	90	0	486	-3	0.22	8	0.6266
			102*	1	102	13	250	-50	0.41	104	0.6315
90	500	0.4	10-250	10	77	-14	1178	136	0.00	-100	0.5533
					91	1	510	2	0.39	-1	0.5532
					96	6	359	-28	0.49	21	0.5482
			90	1	90	0	533	7	0.38	-5	0.5541
			94*	1	94	4	409	-18	0.45	14	0.5498
210	900	0.3	10-250	9	188	-10	1724	92	0.00	-100	1.2455
					210	0	1012	12	0.26	13	1.1660
					243	16	372	-59	0.50	67	1.1440
			210	1	210	0	1008	12	0.26	-13	1.1491
			237*	1	237	13	492	-45	0.45	49	1.1635

Note: *---The Young's modulus derived by Oliver and Pharr's method.

Table 1 Elastic-plastic parameters used in the present study and some simulation results.

Table 2 Examples of parameters obtained from optimisation.

Fig. 1 Schematic illustration of conical indentation and a typical *P-h* response of an elastic-plastic material to instrumented sharp indentation.

Fig. 2 The power law elasto-plastic stress–strain behavior used in the current study.

Fig. 3 Computational modeling of instrumented conical indentation. (a) axisymmetric FE model, (b) the self adaptive mesh and contour of Mises stress at maximum load for E=210 GPa, σ_y=1800 MPa and n=0.5.

Fig. 4 C_e vs E^* relationship for purely elastic materials.

Fig. 5 The relationship between C_{epp_L} (Original) and C_{epp_L} (Predicted).

Fig. 6 FE simulated *P-h* loading curves. P_e---elastic (E=210GPa), P_{ep_L}---elastic-plastic (E=210GPa, σ_y=900MPa, n=0.3), P_{epp_L}---elastic-perfect plastic (E=210GPa, σ_y=900MPa, n=0) materials, Empty cycles---weighted results.

Fig. 7 The relationship between W_L (Original) and W_L (Predicted).

Fig. 8 The best Zeng and Chiu [28] fitting results (lines) to the FE calculated results (symbols) of the upper 50% unloading curves of two materials. The strain hardening exponents are n=0.1 and 0.5 for the same E (210GPa) and σ_y (900MPa).

Fig. 9 The weighting scheme for indentation-unloading curve.

Fig. 10 The fitting results (lines) to the FE calculated results (symbols) of the upper 50% unloading curves of the two materials used in Fig. 8, using the weighting scheme proposed in this paper.

Fig. 11 The overall fitness of the proposed weighting scheme to the unloading curve for the material of E=210GPa, σ_y=900MPa and n=0.5 .

Fig. 12 The relationship between W_{ul} (Original) and W_{ul} (Predicted).

Fig. 13 The relationship between h_r/h_m (Original) and h_r/h_m (Predicted).

Fig. 14 Definitions of objective functions, Eq.(28), for the optimisation.

Fig. 15 Similar P-h curves for several optimised materials corresponding to the original material of E=210GPa, σ_y=900MPa and n=0.3.

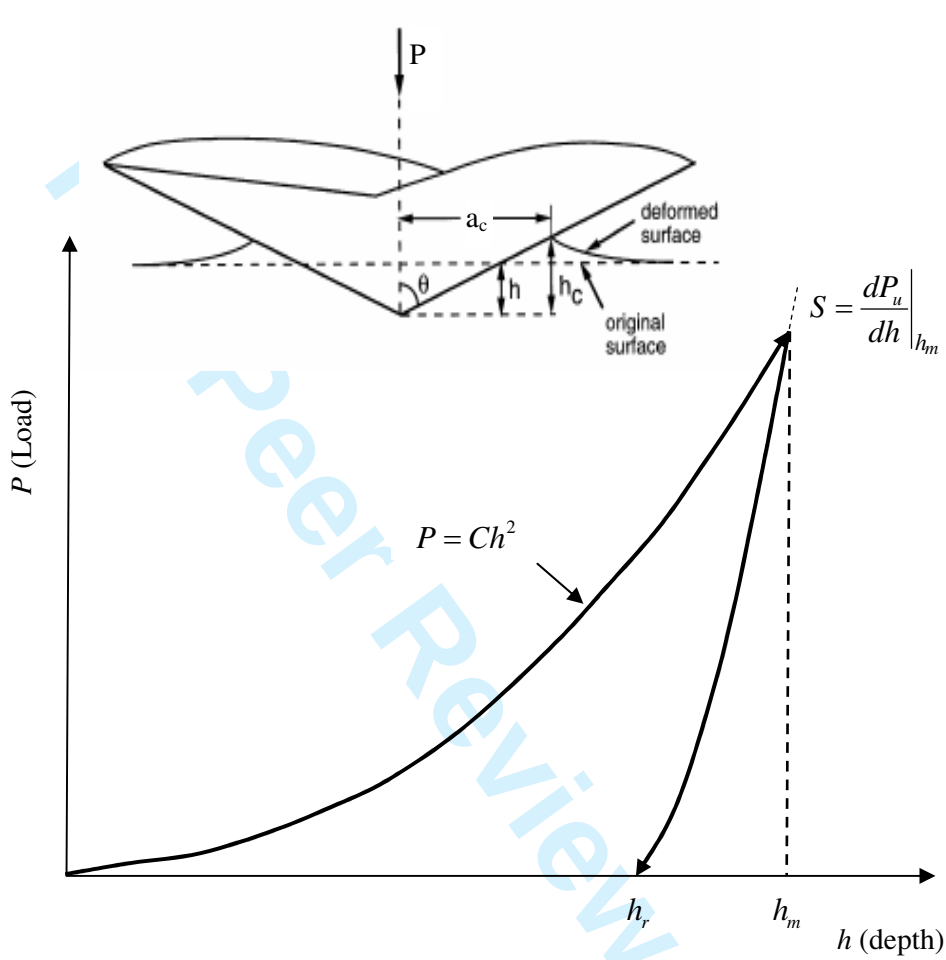

Fig. 1 Schematic illustration of conical indentation and a typical *P*-*h* response of an elastic-plastic material to instrumented sharp indentation.

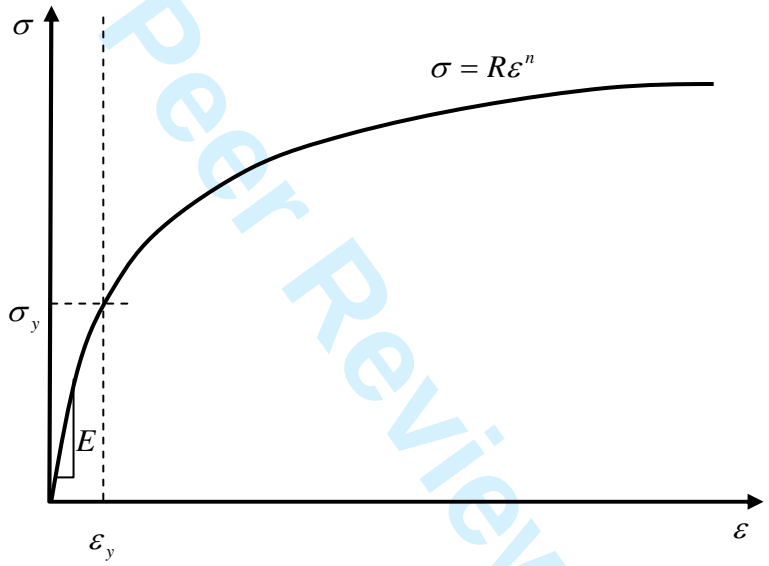

Fig. 2 The power law elasto-plastic stress–strain behavior used in the current study.

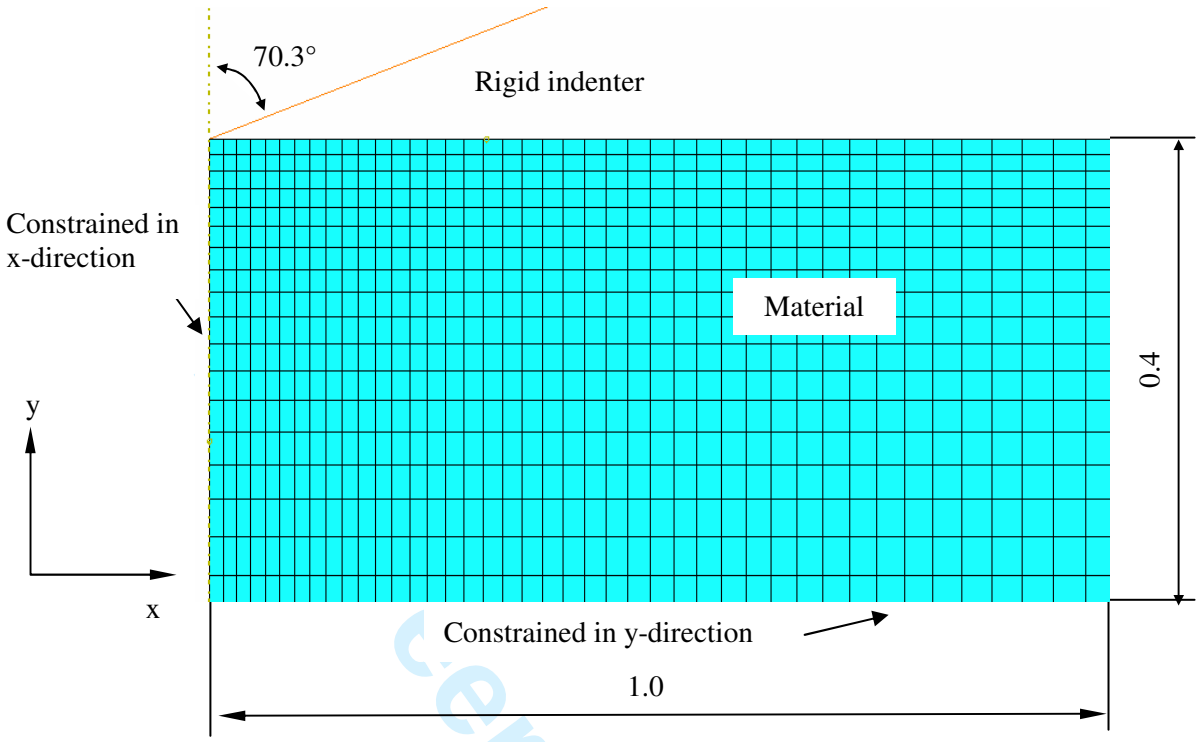

(a)

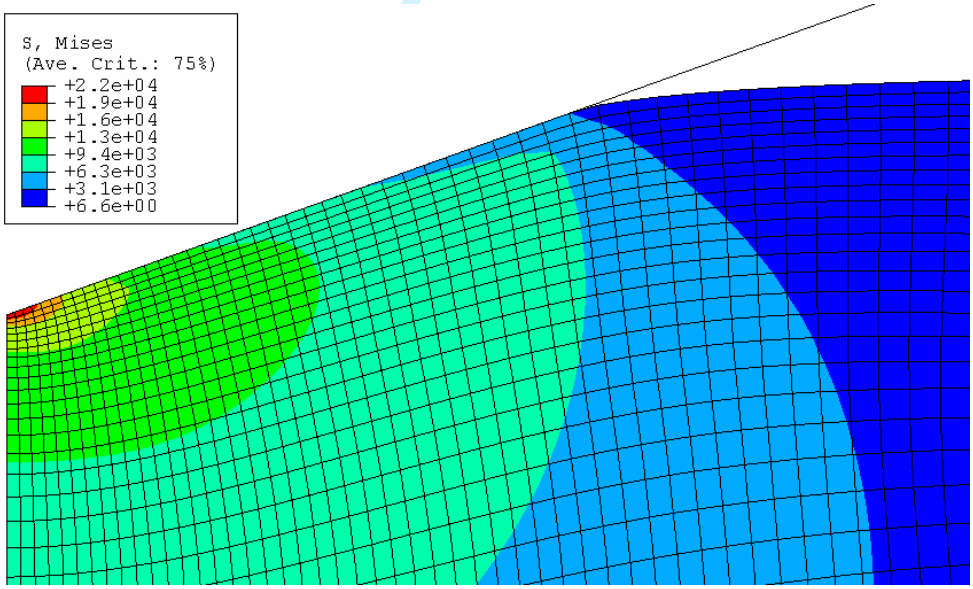

(b)

Fig. 3 Computational modeling of instrumented conical indentation. (a) axisymmetric FE model, (b) the self adaptive mesh and contour of Mises stress at maximum load for E=210 GPa, σ_y=1800 MPa and n=0.5.

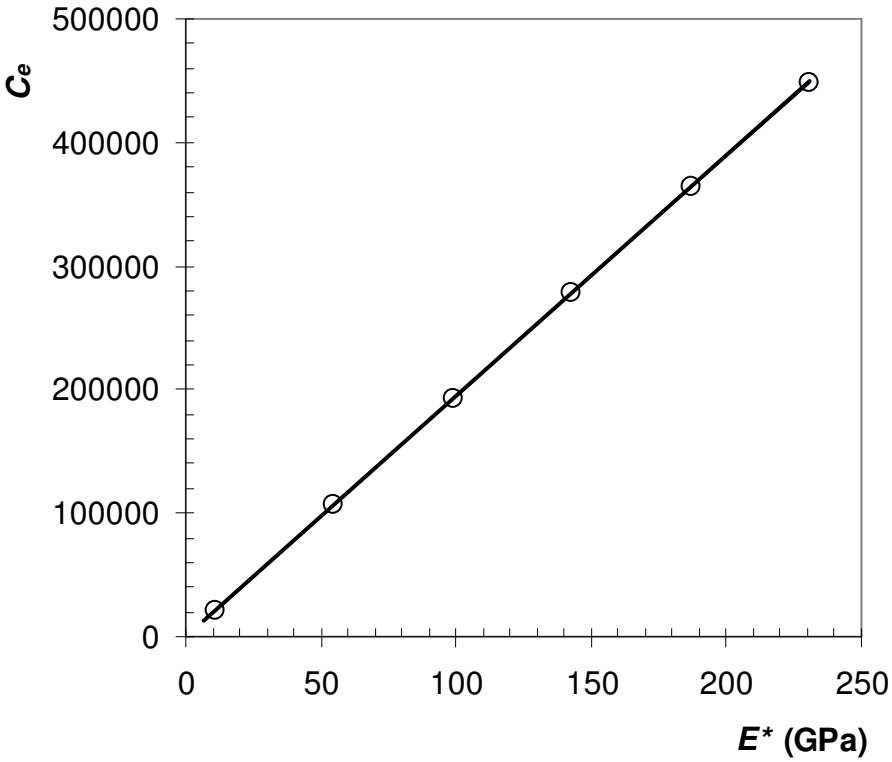

Fig. 4 C_e vs E^* relationship for purely elastic materials.

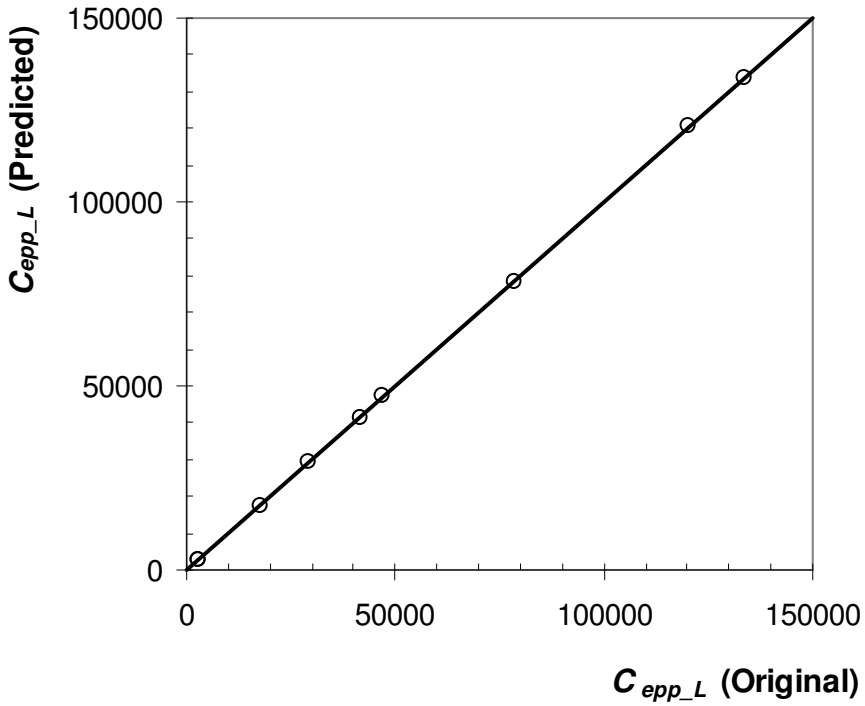

Fig. 5 The relationship between C_{epp_L} (Original) and C_{epp_L} (Predicted).

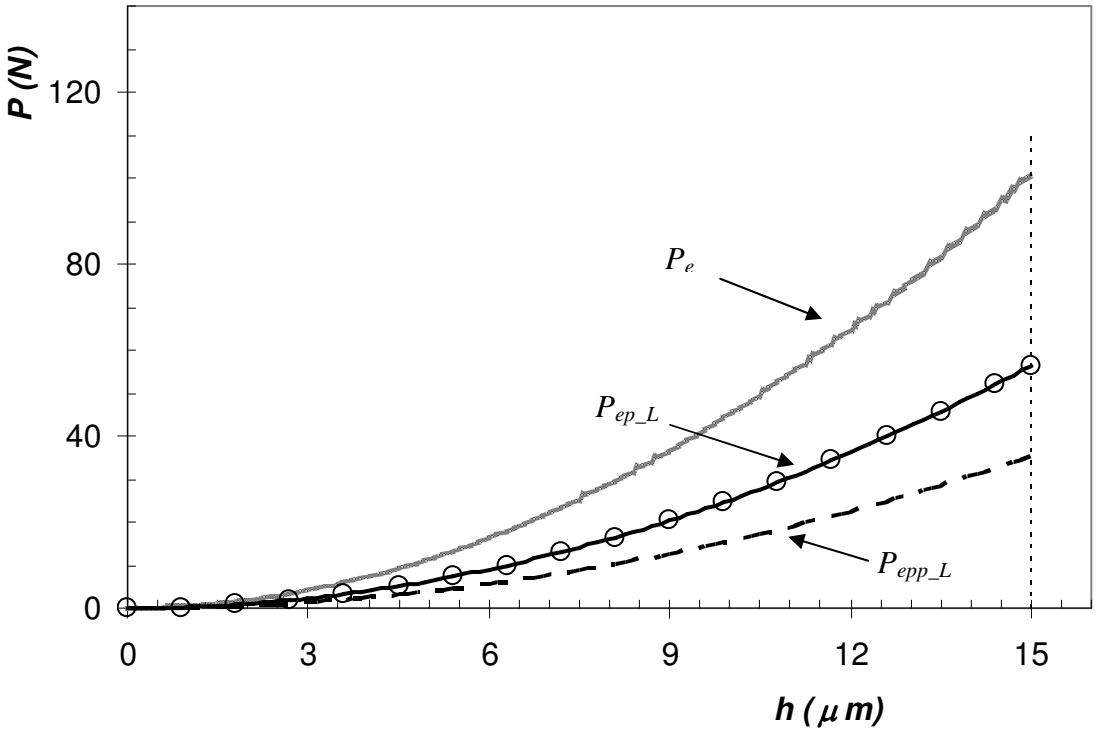

Fig. 6 FE simulated *P*-*h* loading curves. P_e---elastic (E=210GPa), P_{ep_L}---elastic-plastic (E=210GPa, σ_y=900MPa, n=0.3), P_{epp_L}---elastic-perfect plastic (E=210GPa, σ_y=900MPa, n=0) materials, Empty cycles---weighted results.

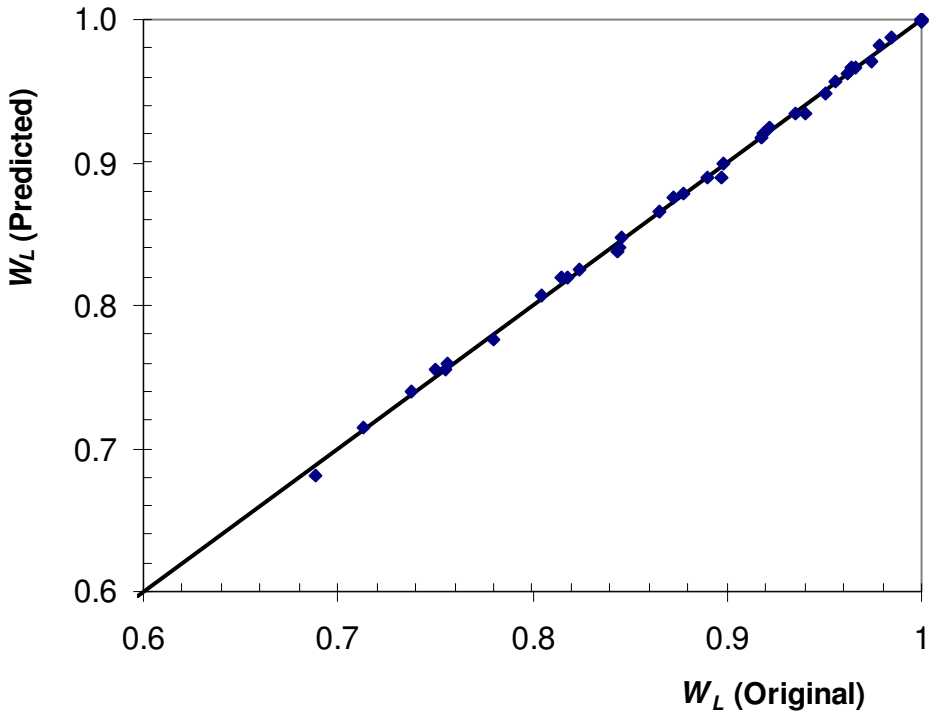

Fig. 7 The relationship between W_L (Original) and W_L (Predicted).

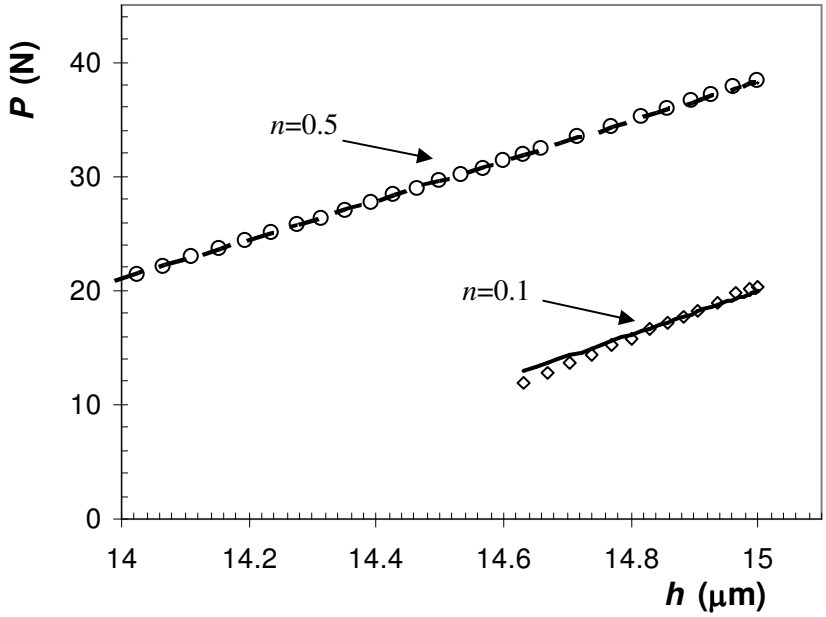

Fig. 8 The best Zeng and Chiu [28] fitting results (lines) to the FE calculated results (symbols) of the upper 50% unloading curves of two materials. The strain hardening exponents are n=0.1 and 0.5 for the same E (210GPa) and σ_y (900MPa).

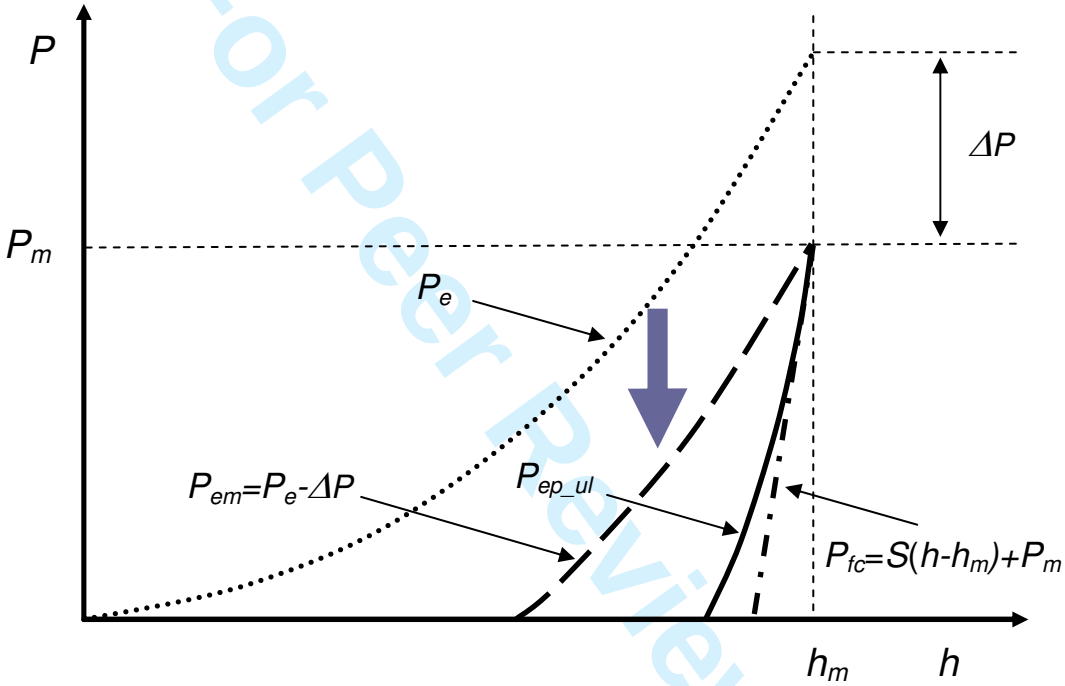

Fig. 9 The weighting scheme for indentation-unloading curve.

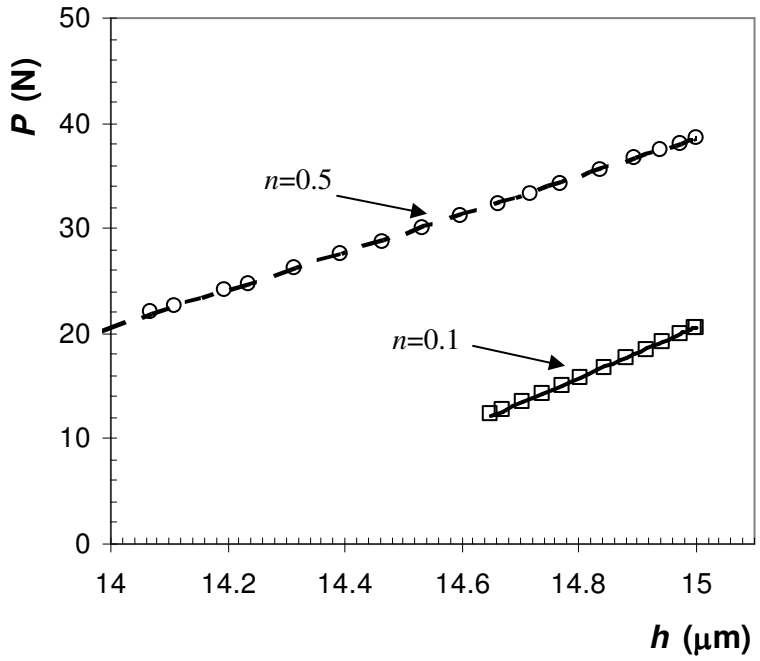

Fig. 10 The fitting results (lines) to the FE calculated results (symbols) of the upper 50% unloading curves of the two materials used in Fig. 8, using the weighting scheme proposed in this paper.

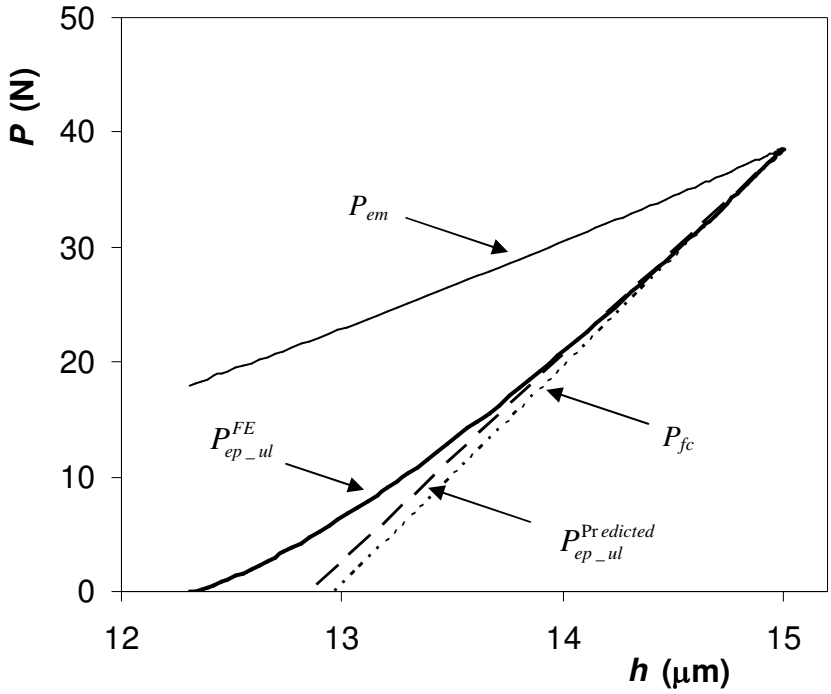

Fig. 11 The overall fitness of the proposed weighting scheme to the unloading curve for the material of E=210GPa, σ_y=900MPa and n=0.5 .

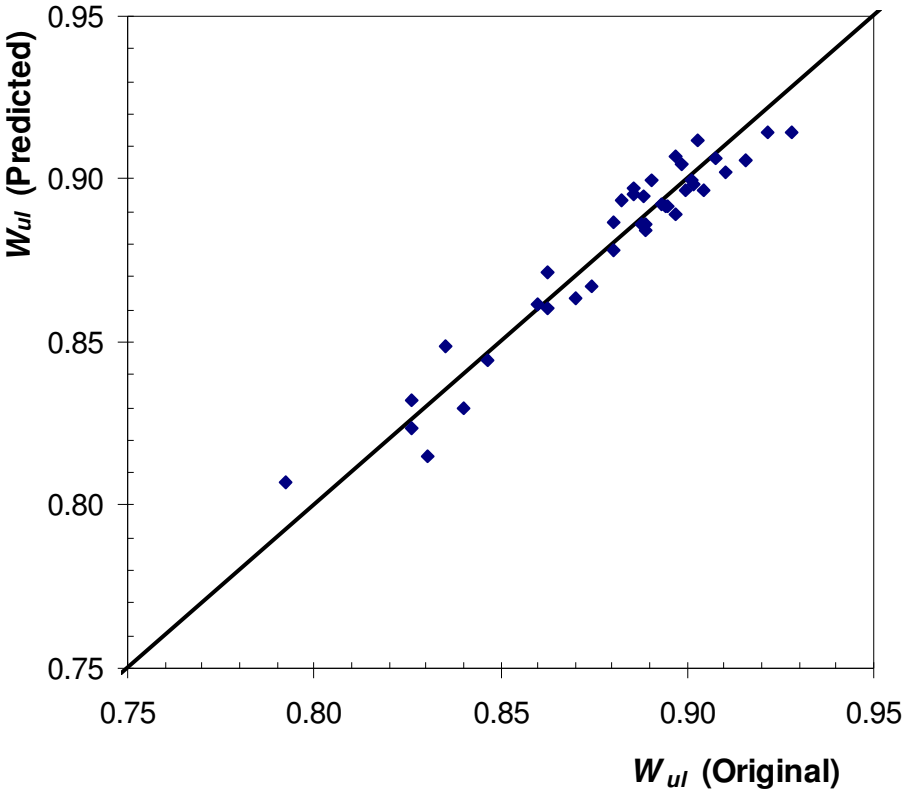

Fig. 12 The relationship between W_{ul} (Original) and W_{ul} (Predicted).

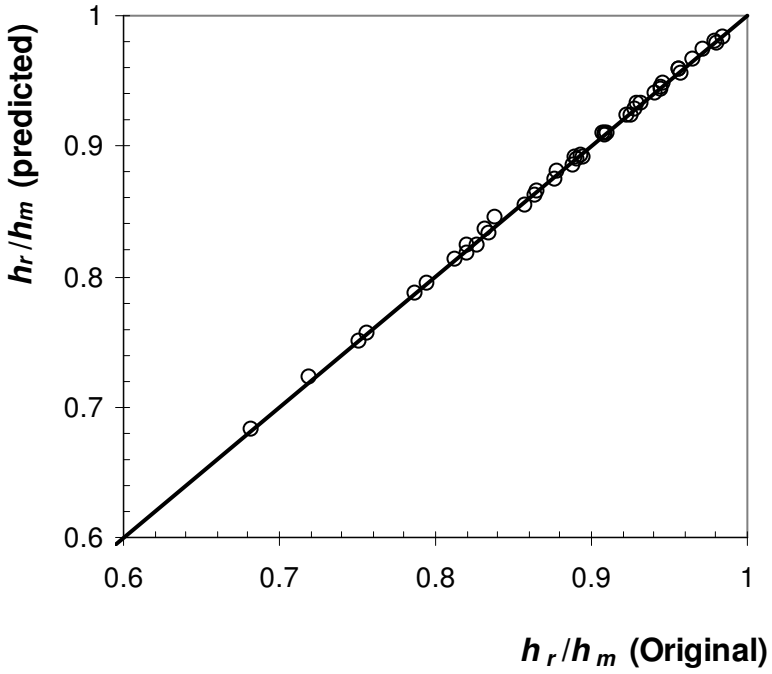

Fig. 13 The relationship between h_r/h_m (Original) and h_r/h_m (Predicted).

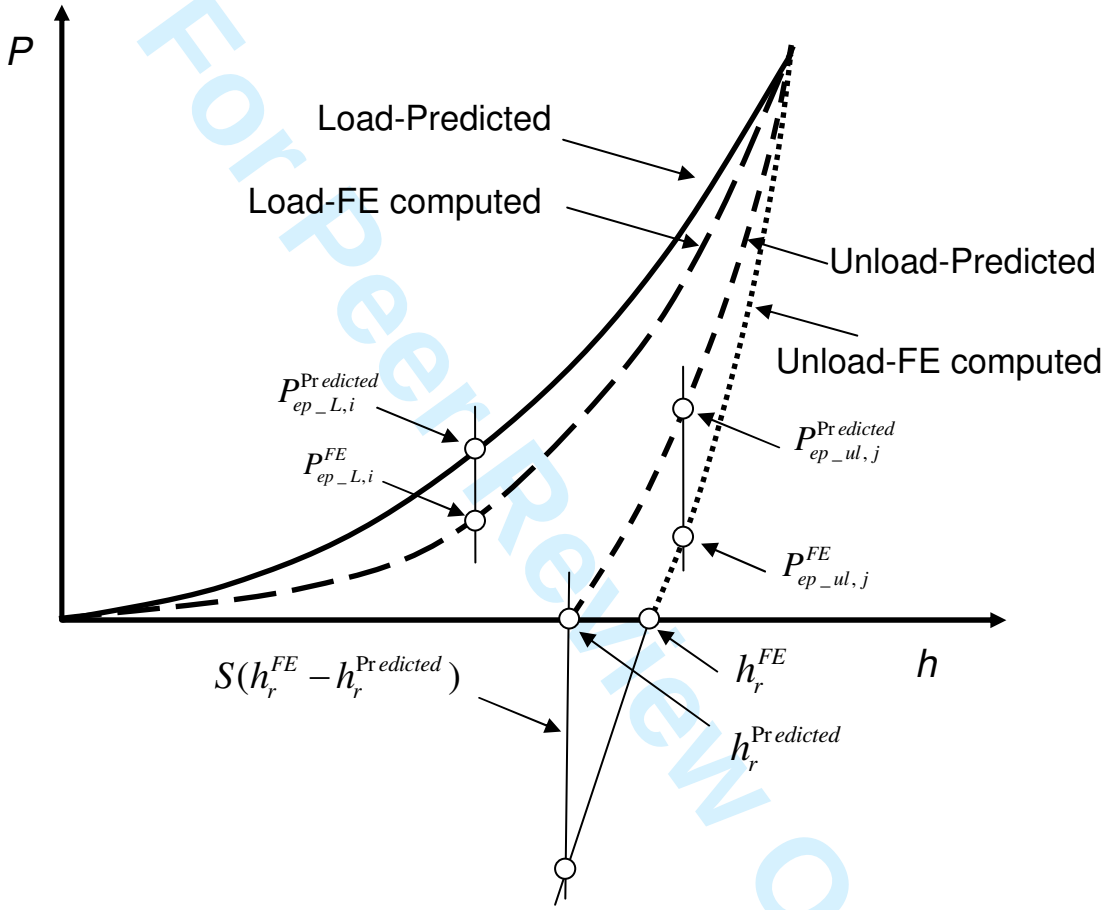

Fig. 14 Definitions of objective functions, Eq.(28), for the optimisation.

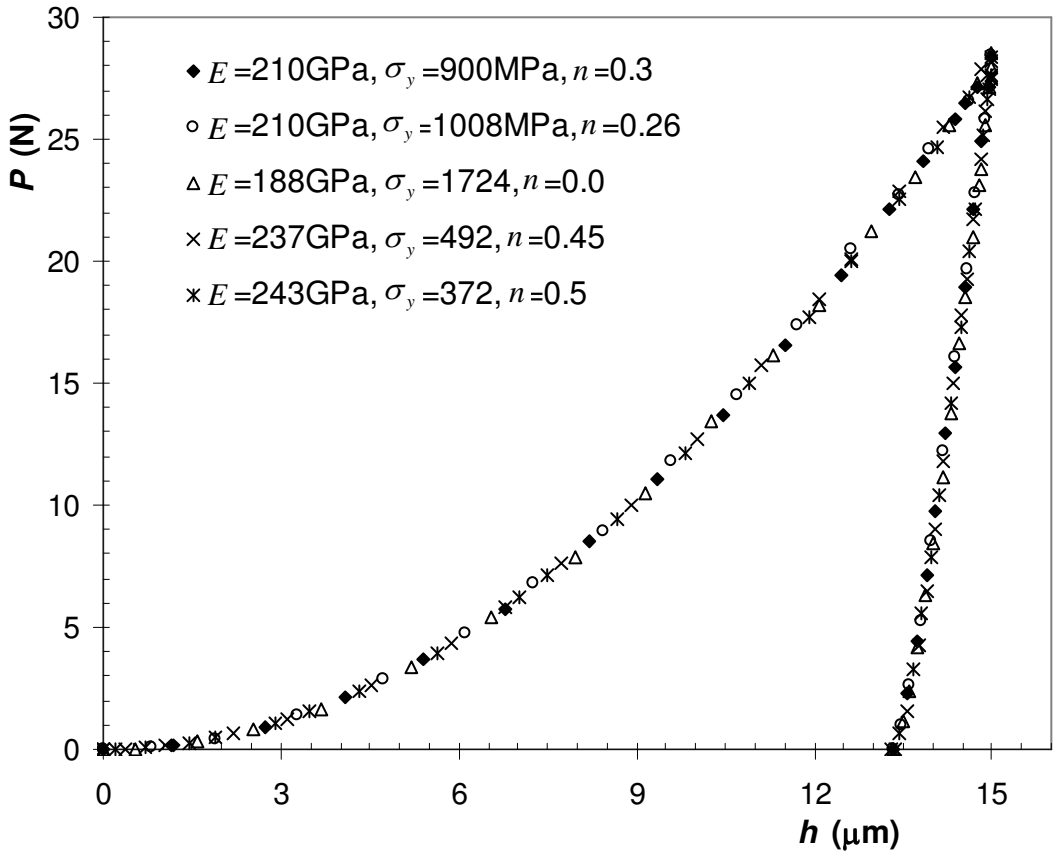

Fig. 15 Similar *P-h* curves for several optimised materials corresponding to the original material of E=210GPa, σ_y=900MPa and n=0.3.

Table 1 Elastic-plastic parameters used in the present study and some simulation results.

Table 2 Examples of parameters obtained from optimisation.

Fig. 1 Schematic illustration of conical indentation and a typical *P-h* response of an elastic-plastic material to instrumented sharp indentation.

Fig. 2 The power law elasto-plastic stress–strain behavior used in the current study.

Fig. 3 Computational modeling of instrumented conical indentation. (a) axisymmetric FE model, (b) the self adaptive mesh and contour of Mises stress at maximum load for E=210 GPa, σ_y=1800 MPa and n=0.5.

Fig. 4 C_e vs E^* relationship for purely elastic materials.

Fig. 5 The relationship between C_{epp_L} (Original) and C_{epp_L} (Predicted).

Fig. 6 FE simulated *P-h* loading curves. P_e---elastic (E=210GPa), P_{ep_L}---elastic-plastic (E=210GPa, σ_y=900MPa, n=0.3), P_{epp_L}---elastic-perfect plastic (E=210GPa, σ_y=900MPa, n=0) materials, Empty cycles---weighted results.

Fig. 7 The relationship between W_L (Original) and W_L (Predicted).

Fig. 8 The best Zeng and Chiu [**Error! Bookmark not defined.**] fitting results (lines) to the FE calculated results (symbols) of the upper 50% unloading curves of two materials. The strain hardening exponents are n=0.1 and 0.5 for the same E (210GPa) and σ_y (900MPa).

Fig. 9 The weighting scheme for indentation-unloading curve.

Fig. 10 The fitting results (lines) to the FE calculated results (symbols) of the upper 50% unloading curves of the two materials used in Fig. 8, using the weighting scheme proposed in this paper.

Fig. 11 The overall fitness of the proposed weighting scheme to the unloading curve for the material of E=210GPa, σ_y=900MPa and n=0.5 .

Fig. 12 The relationship between W_{ul} (Original) and W_{ul} (Predicted).

Fig. 13 The relationship between h_r/h_m (Original) and h_r/h_m (Predicted).

Fig. 14 Definitions of objective functions, Eq.(28), for the optimisation.

Fig. 15 Similar P-h curves for several optimised materials corresponding to the original material of E=210GPa, σ_y=900MPa and n=0.3.

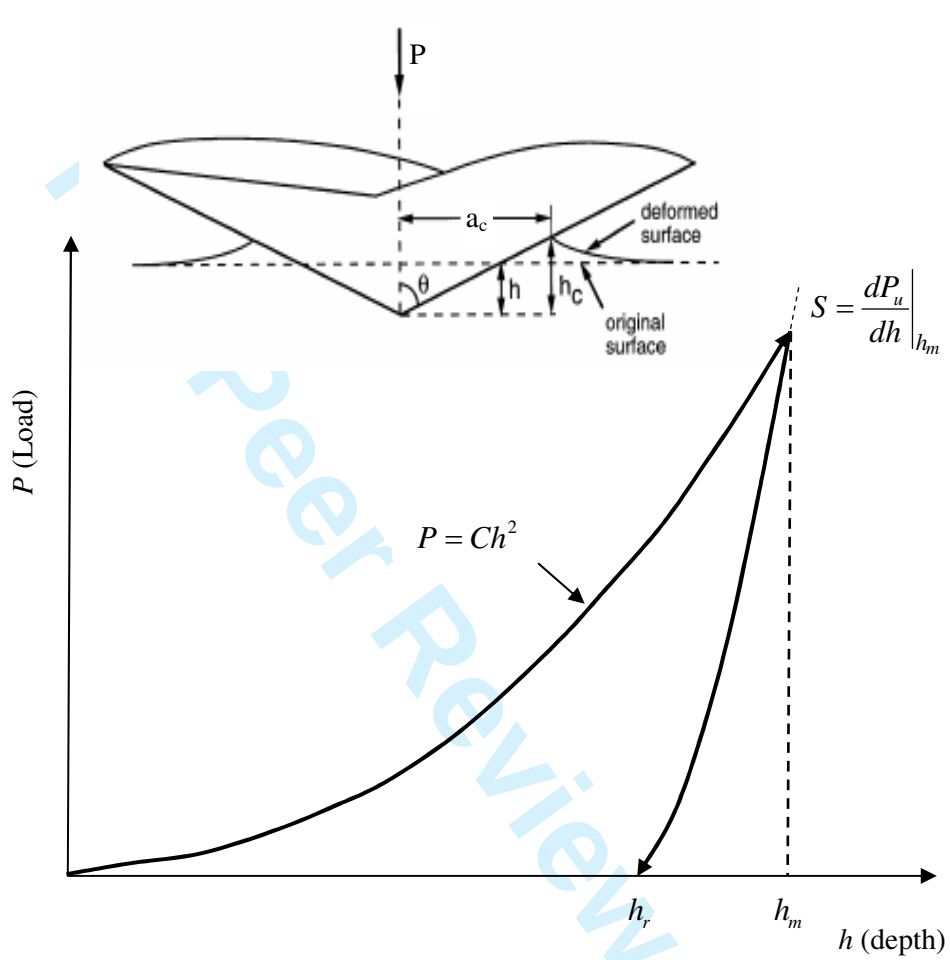

Fig. 1 Schematic illustration of conical indentation and a typical *P*-*h* response of an elastic-plastic material to instrumented sharp indentation.

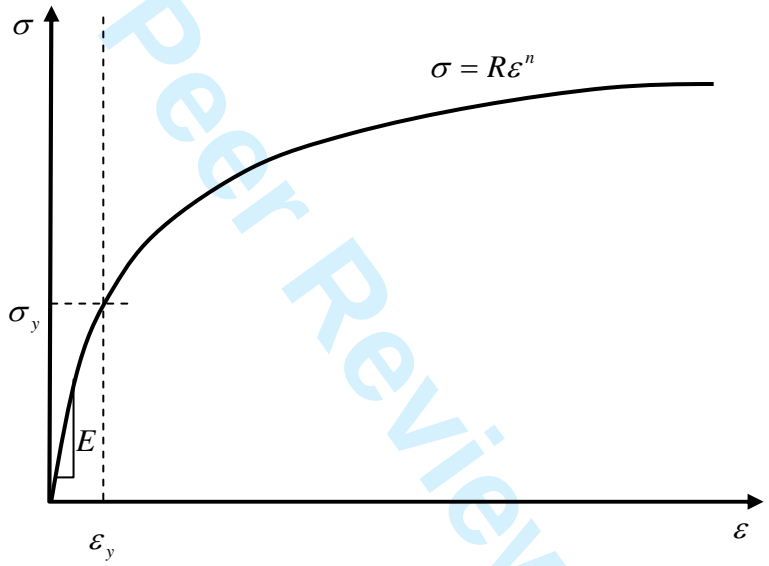

Fig. 2 The power law elasto-plastic stress–strain behavior used in the current study.

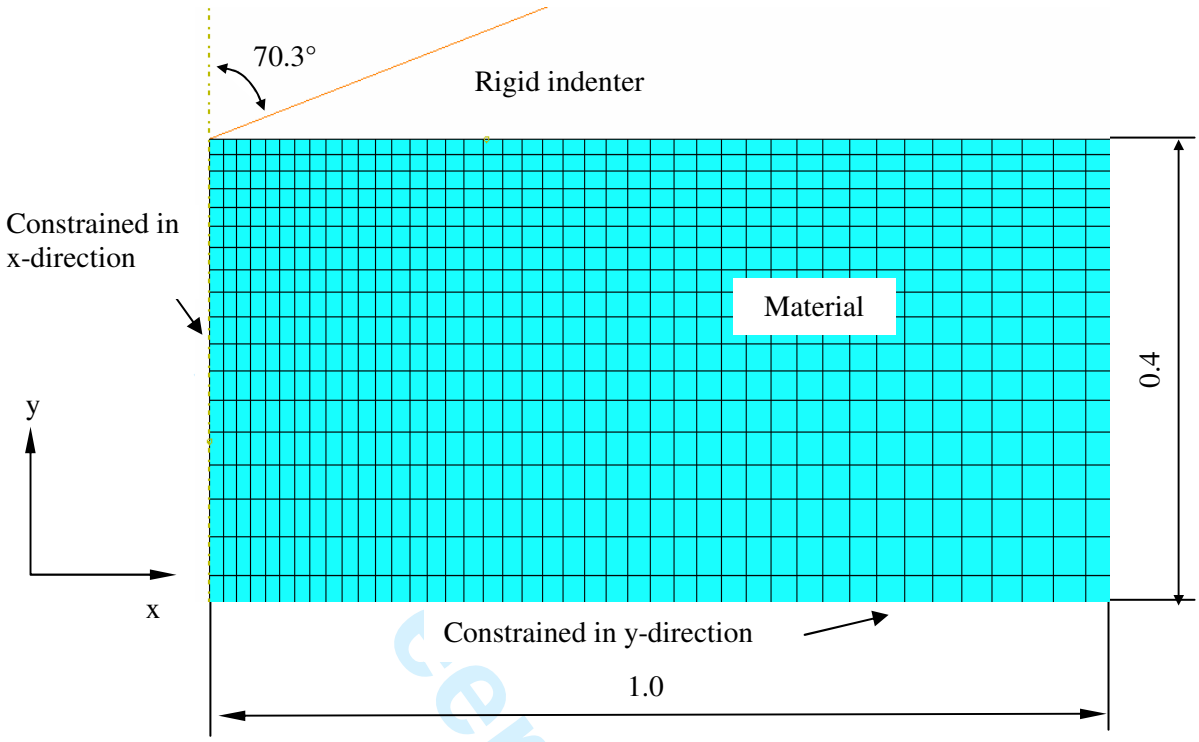

(a)

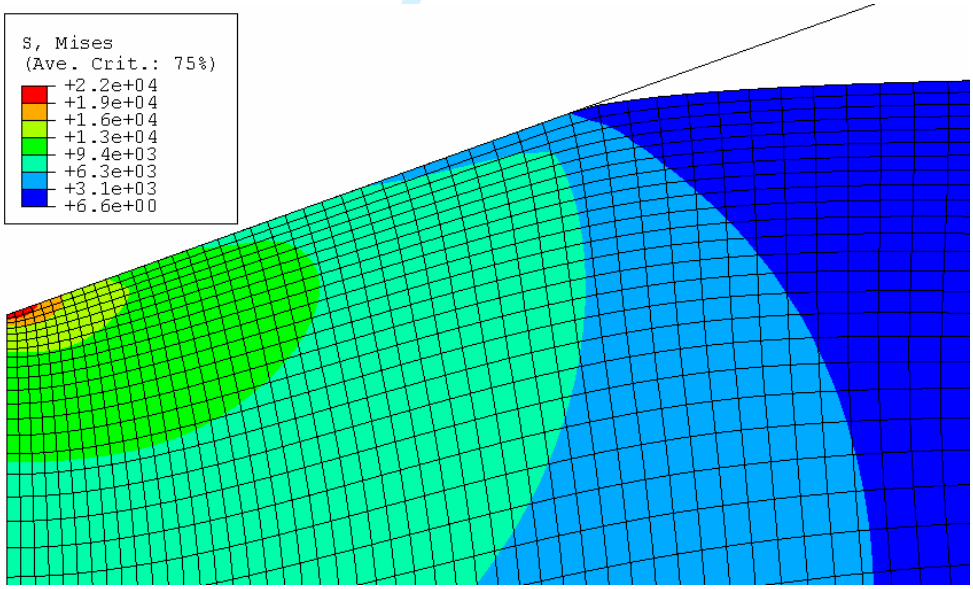

(b)

Fig. 3 Computational modeling of instrumented conical indentation. (a) axisymmetric FE model, (b) the self adaptive mesh and contour of Mises stress at maximum load for E=210 GPa, σ_y=1800 MPa and n=0.5.

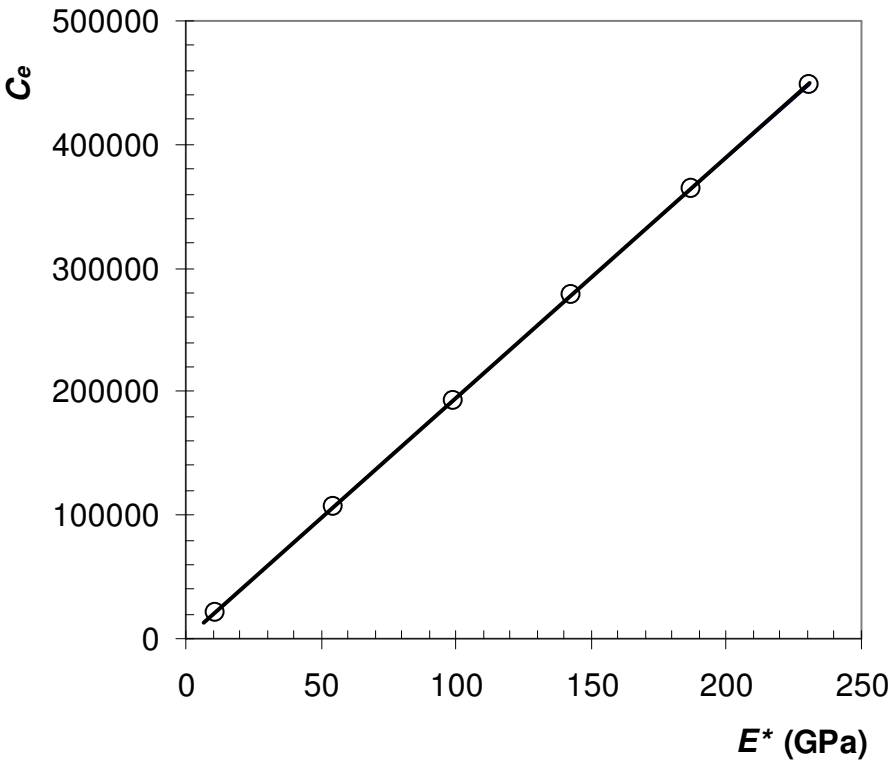

Fig. 4 C_e vs E^* relationship for purely elastic materials.

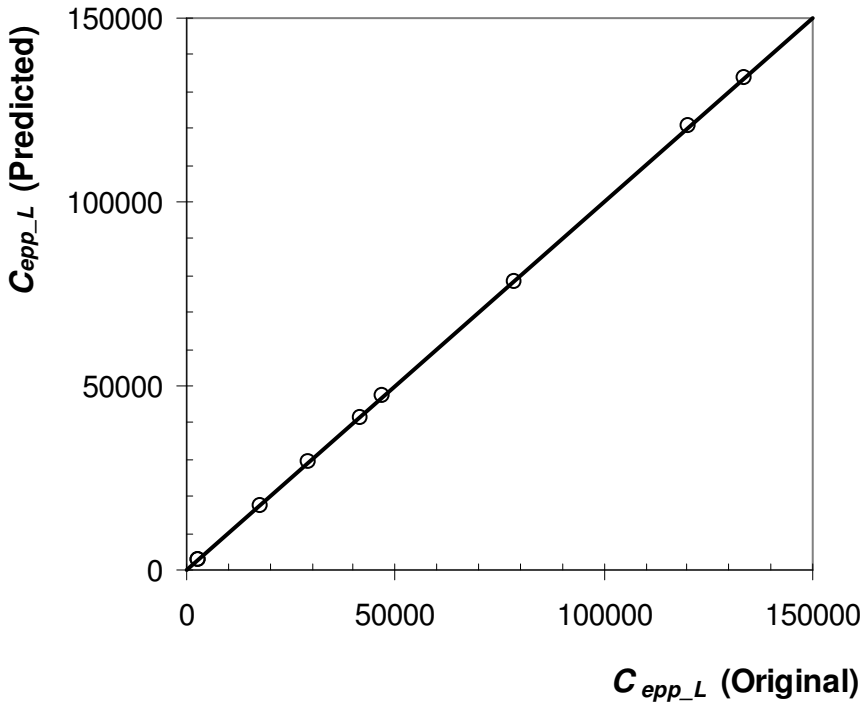

Fig. 5 The relationship between C_{epp_L} (Original) and C_{epp_L} (Predicted).

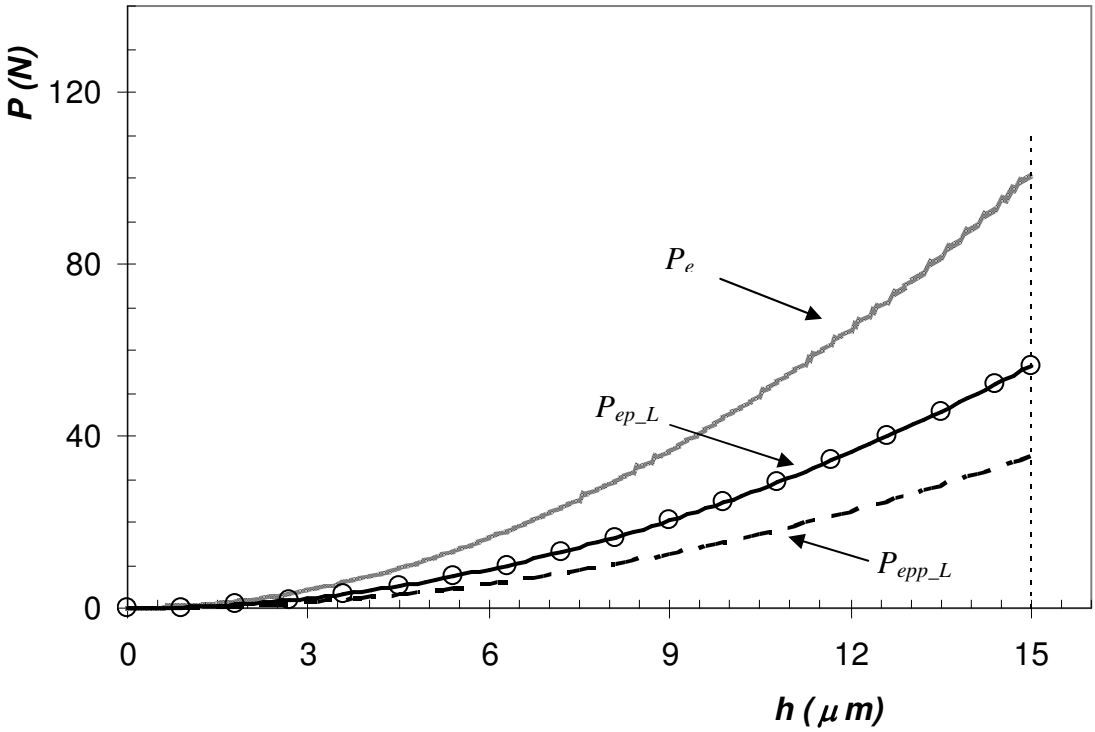

Fig. 6 FE simulated *P*-*h* loading curves. P_e---elastic (E=210GPa), P_{ep_L}---elastic-plastic (E=210GPa, σ_y=900MPa, n=0.3), P_{epp_L}---elastic-perfect plastic (E=210GPa, σ_y=900MPa, n=0) materials, Empty cycles---weighted results.

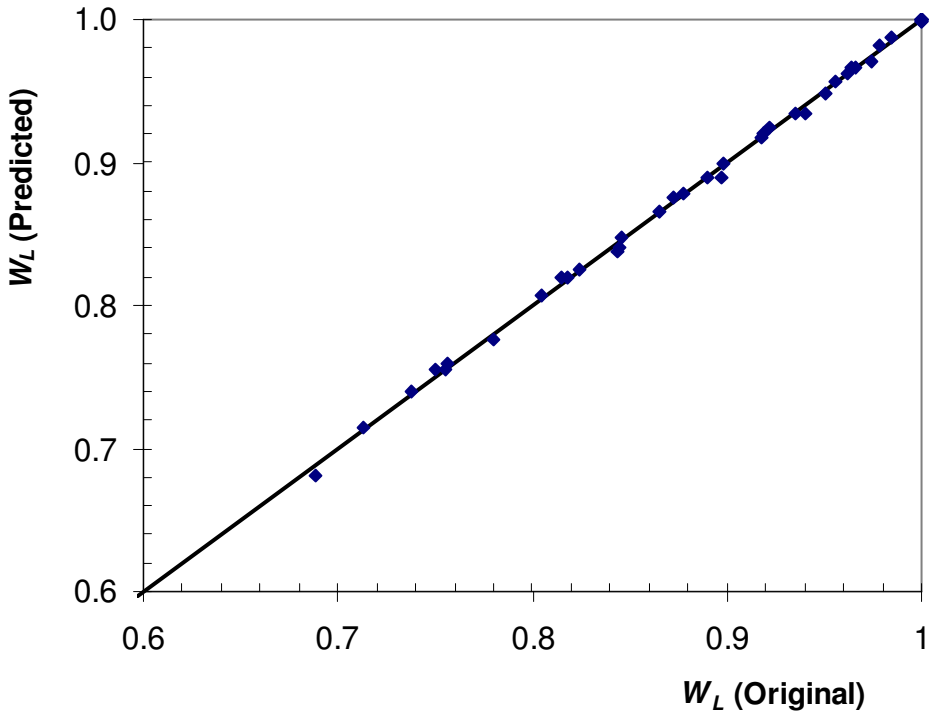

Fig. 7 The relationship between W_L (Original) and W_L (Predicted).

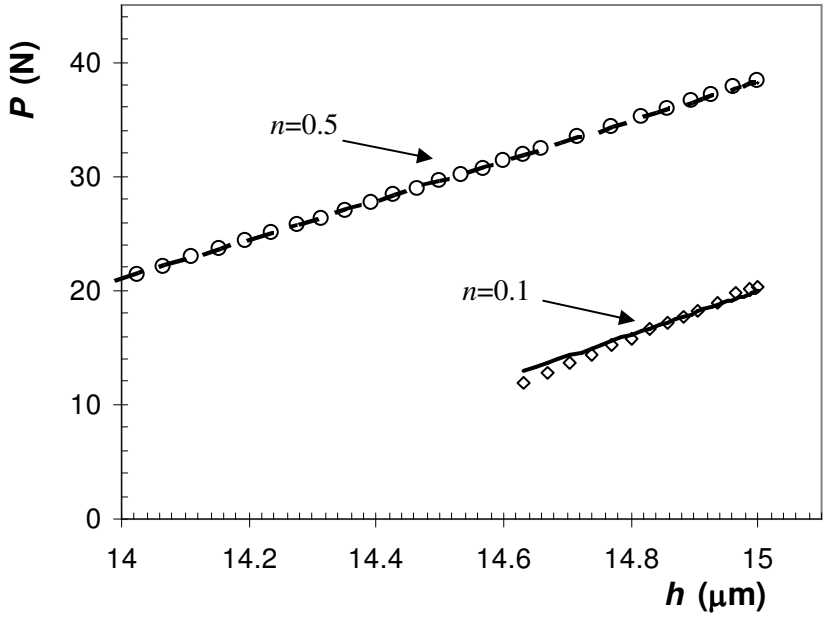

Fig. 8 The best Zeng and Chiu [**Error! Bookmark not defined.**] fitting results (lines) to the FE calculated results (symbols) of the upper 50% unloading curves of two materials. The strain hardening exponents are n=0.1 and 0.5 for the same E (210GPa) and σ_y (900MPa).

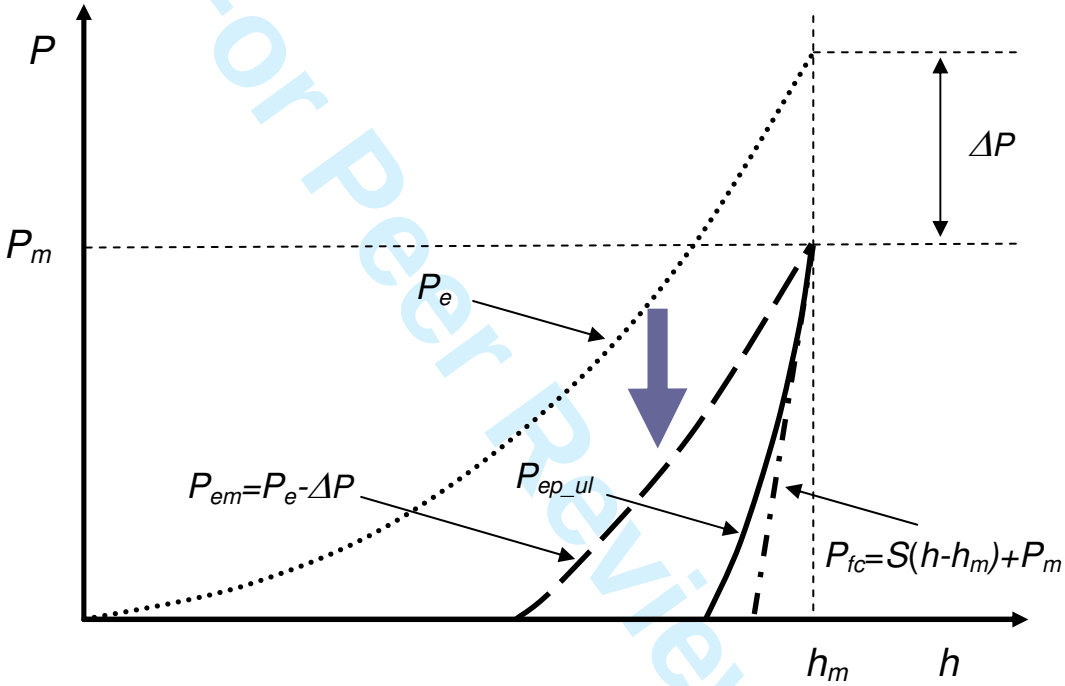

Fig. 9 The weighting scheme for indentation-unloading curve.

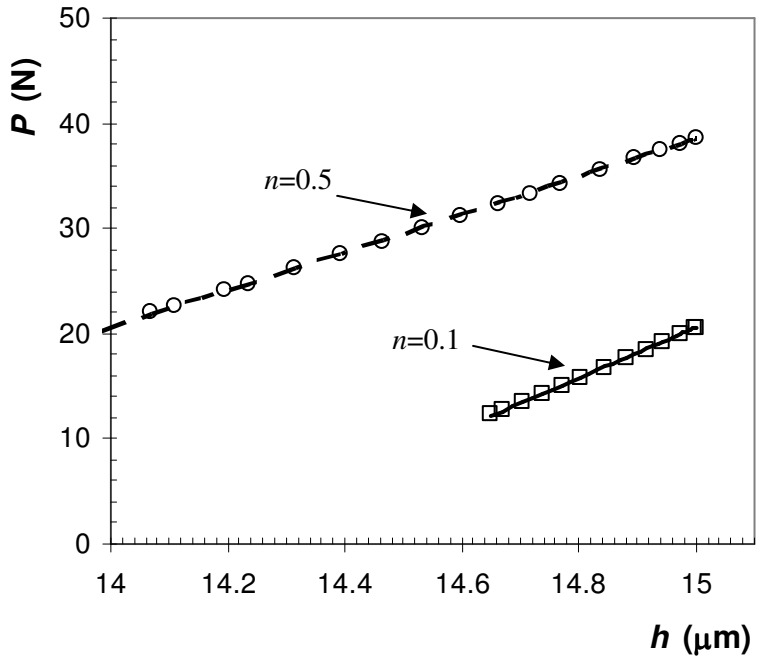

Fig. 10 The fitting results (lines) to the FE calculated results (symbols) of the upper 50% unloading curves of the two materials used in Fig. 8, using the weighting scheme proposed in this paper.

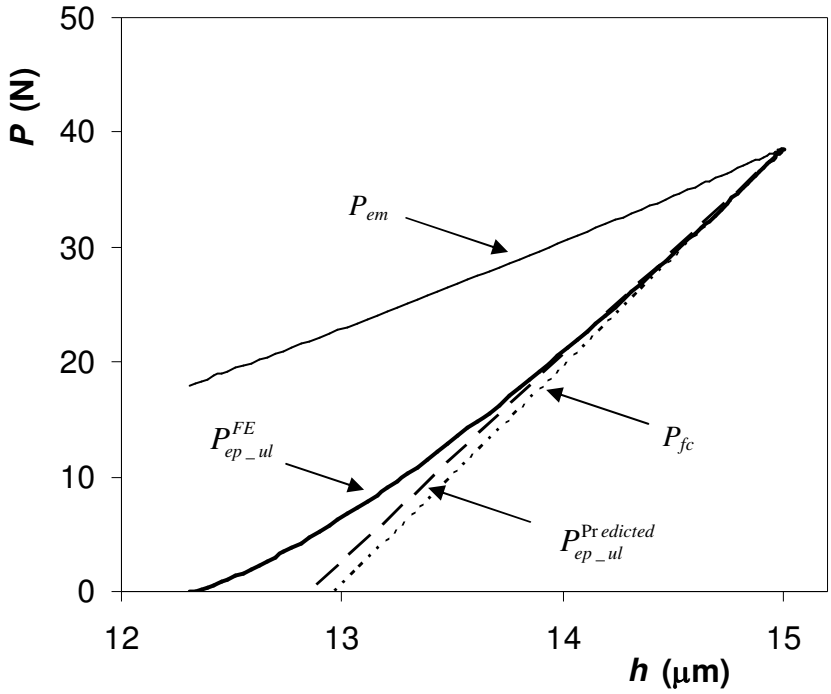

Fig. 11 The overall fitness of the proposed weighting scheme to the unloading curve for the material of E=210GPa, σ_y=900MPa and n=0.5 .

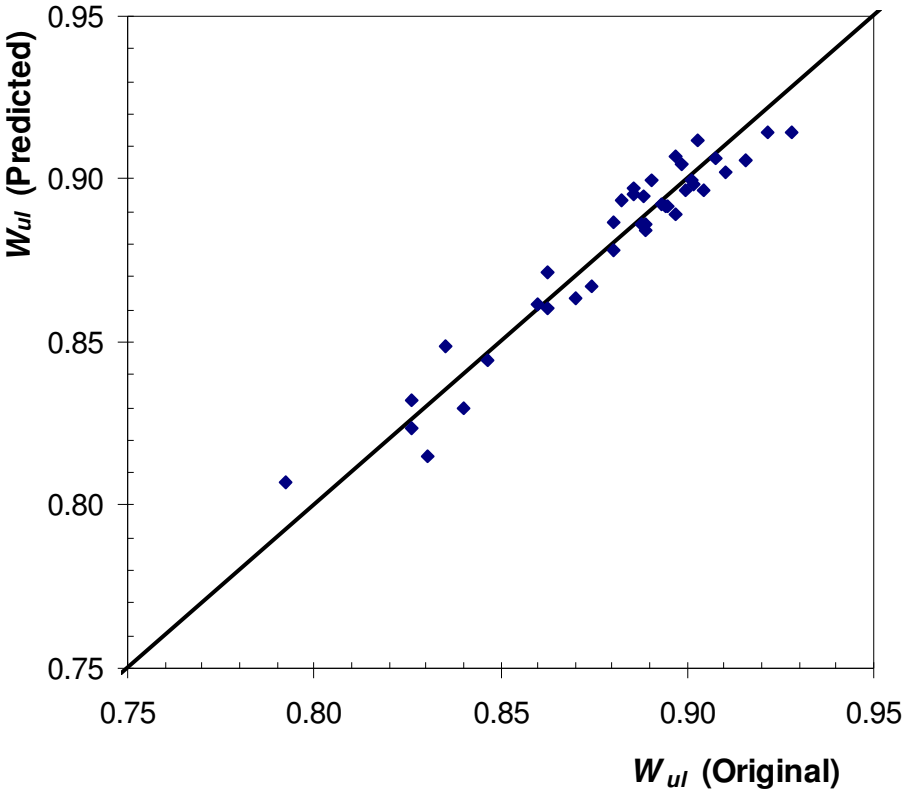

Fig. 12 The relationship between W_{ul} (Original) and W_{ul} (Predicted).

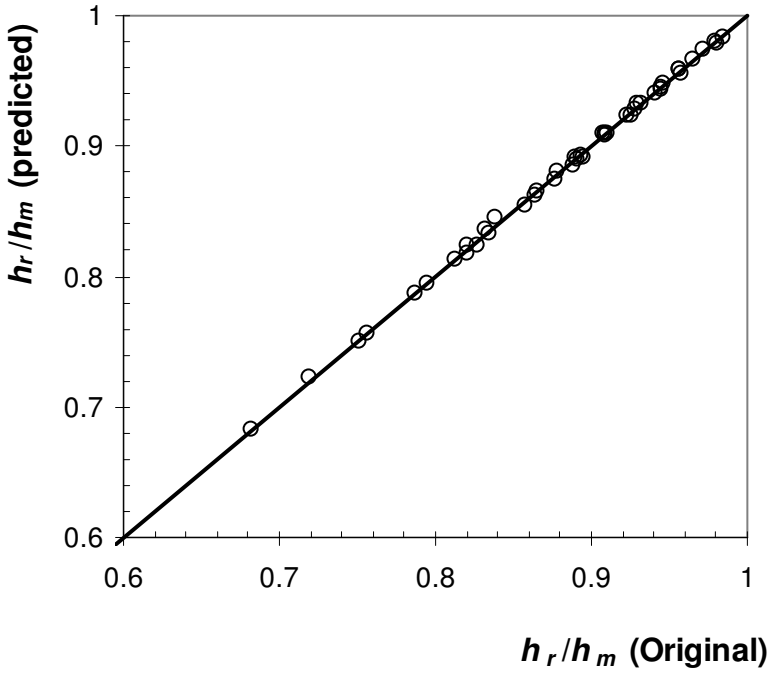

Fig. 13 The relationship between h_r/h_m (Original) and h_r/h_m (Predicted).

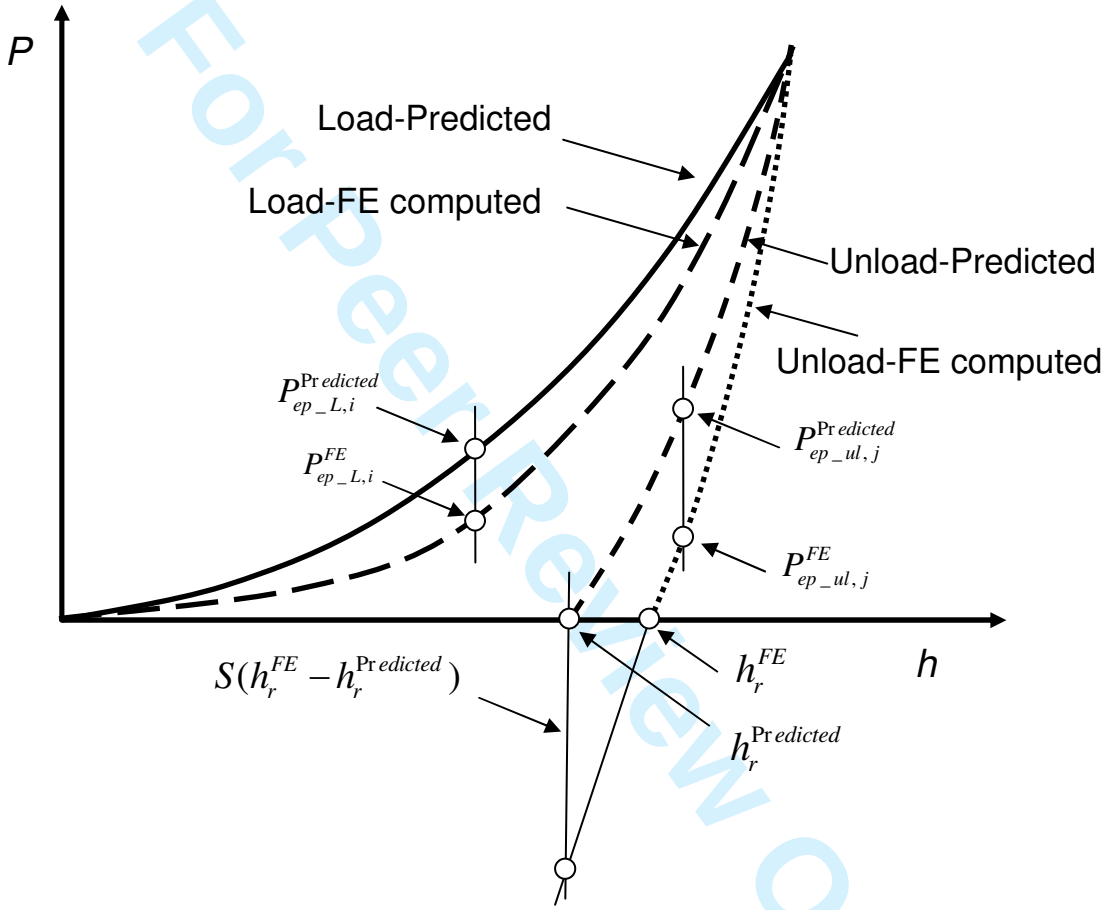

Fig. 14 Definitions of objective functions, Eq.(28), for the optimisation.

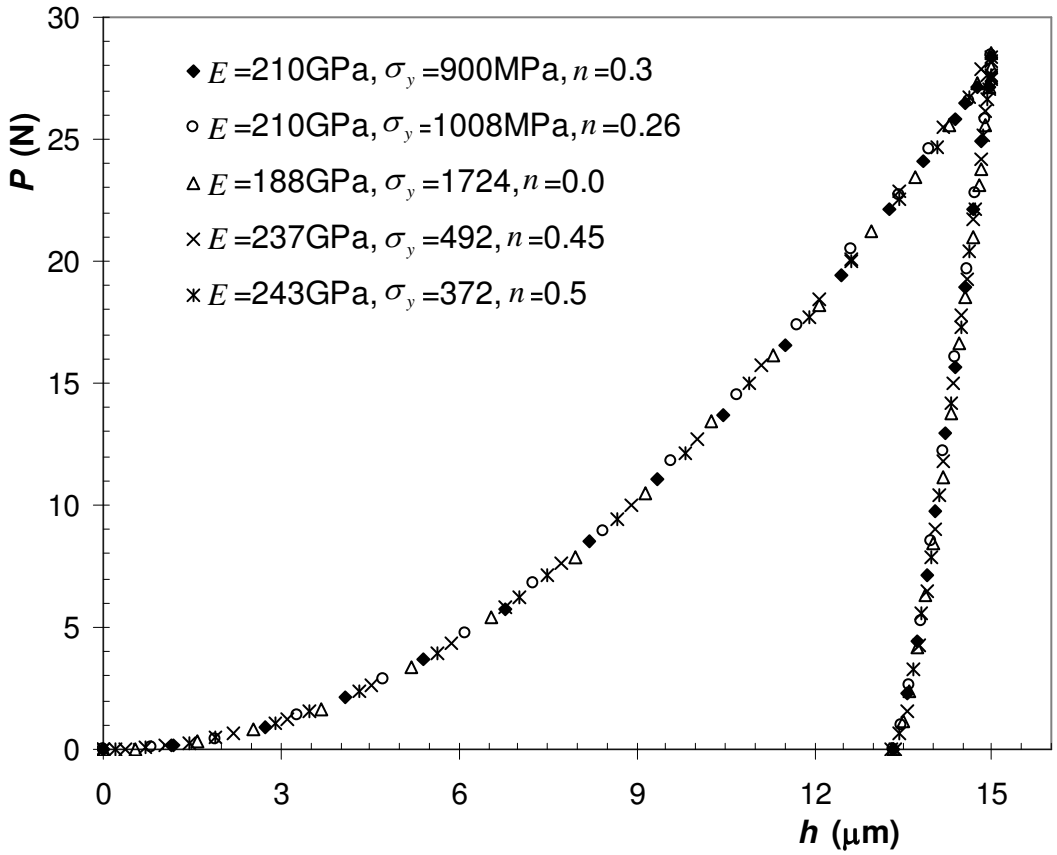

Fig. 15 Similar *P-h* curves for several optimised materials corresponding to the original material of E=210GPa, σ_y=900MPa and n=0.3.